GRAPH TOKENIZATION FOR BRIDGING GRAPHS AND TRANSFORMERS

Anonymous authors
Paper under double-blind review

ABSTRACT

The success of large pretrained Transformers is closely tied to tokenizers, which convert raw input into discrete symbols. Extending these models to graph-structured data remains a significant challenge. In this work, we introduce a graph tokenization framework that generates sequential representations of graphs by combining reversible graph serialization, which preserves graph information, with Byte Pair Encoding (BPE), a widely adopted tokenizer in large language models (LLMs). To better capture structural information, the graph serialization process is guided by global statistics of graph substructures, ensuring that frequently occurring substructures appear more often in the sequence and can be merged by BPE into meaningful tokens. Empirical results demonstrate that the proposed tokenizer enables Transformers such as BERT to be directly applied to graph benchmarks without architectural modifications. The proposed approach achieves state-of-the-art results on 14 benchmark datasets and frequently outperforms both graph neural networks and specialized graph transformers. This work bridges the gap between graph-structured data and the ecosystem of sequence models.

1 INTRODUCTION

Large pretrained Transformer models (Vaswani et al., 2017; Minaee et al., 2024), exemplified by LLMs, have achieved state-of-the-art results across diverse domains (Dosovitskiy et al., 2020; Gong et al., 2021). A key component of this success is the tokenizer, which converts raw input into sequences of discrete symbols. By structuring information into learnable units, the tokenizer provides the interface between complex data and Transformer architectures, supporting the scalability and performance of these models.

Research on extending Transformers to graph-structured data has explored two main strategies, each with inherent limitations (Yu et al., 2025). One strategy modifies the architecture by incorporating attention mechanisms into Graph Neural Networks (GNNs) to create specialized Graph Transformers (Yun et al., 2019). These approaches require graph-specific designs that diverge from standard sequence models and their ecosystem. The other strategy converts graphs into continuous embeddings for use with Transformers (Tang et al., 2024), but this often causes information loss or unstable representations, which can degrade model performance (Chen et al., 2024).

Developing a principled graph tokenizer requires reexamining the notion of tokenization in the context of graph-structured data. Specifically, text can be modeled as a path graph, where the linear sequence of tokens provides both a fixed neighborhood structure and a canonical ordering, making tokenization relatively straightforward. In contrast, general graphs pose additional challenges, as their neighborhoods can branch in multiple directions rather than follow a simple linear sequence. They also lack permutation invariance, where graphs under node permutations are considered equivalent. Furthermore, co-occurrence statistics widely used in text, such as n-gram frequencies based on contiguous tokens, are not directly applicable to graphs.

We propose a framework that addresses these challenges by integrating graph serialization with Byte Pair Encoding (BPE), a data-driven compression algorithm widely applied in text tokenization (Shibata et al., 1999). To ensure that graph structure and labels are preserved, we adopt reversible serialization methods such as extended Euler circuits and minimal-weight graph traversals. Ordering ambiguity is resolved by using global statistics to deterministically guide the serialization process, which translates common substructures into frequent and adjacent symbol patterns that BPE is well suited to merge. Specifically, BPE iteratively merges the most frequent pairs of symbols into new tokens, thereby reducing sequence length while preserving common substructures. As a result,

applying BPE to serialized graphs enables the construction of a vocabulary of frequent graph neighborhoods, producing discrete tokens that are both informative and well aligned with Transformer architectures.

In this work, our contributions can be summarized as follows:

- **General Framework for Graph Tokenization.** We introduce a tokenization framework that combines reversible graph serialization with BPE. By decoupling the encoding of graph structure from the model architecture, this framework provides an effective interface that enables standard off-the-shelf Transformer models to be applied directly to graph-structured data without requiring any architectural modifications.
- **Structure-Guided Serialization for BPE.** We propose a deterministic serialization process guided by global statistics of graph substructures. The process addresses ordering ambiguities in graphs and aligns frequently occurring substructures into adjacent sequence patterns. Structure-Guided Serialization provides an effective basis for BPE to learn a meaningful and interpretable vocabulary of structural graph tokens.
- **State-of-the-Art Performance on Downstream Tasks.** Our tokenizer enables standard Transformer backbones to achieve state-of-the-art results across a diverse suite of 14 benchmarks for graph classification and regression. The proposed approach frequently outperforms both established Graph Neural Networks and specialized Graph Transformers, demonstrating its effectiveness and generalization.

2 Related Works

Graph Neural Networks. Graph Neural Networks (Kipf, 2016; Luo et al., 2025) are the prevailing framework for learning on graph-structured data. They rely on message passing, where node representations are updated by iteratively aggregating information from local neighbors, enabling effective modeling of local graph structure (Chen et al., 2019). To capture dependencies beyond local neighborhoods, subsequent work introduced self-attention, leading to Graph Transformers (Yun et al., 2019; Wu et al., 2023)and hybrid global-local models (He et al., 2023; Zhang et al., 2023). More recently, graph representation learning has been combined with Graph Foundation Models, often by mapping graph structure and features into the embedding space of pretrained LLMs (Tang et al., 2024; Chen et al., 2024). These approaches depend on cross-modal alignment, with performance influenced by the semantic compatibility between graph features and natural language. Our objective is to design an interface that enables graphs to be processed directly by standard, off-the-shelf Transformers.

Graph Serialization. Serialization of a graph into a sequence was one of the earliest strategies for applying sequence-based models. Early methods such as DeepWalk generated node sequences through random walks and processed them with shallow neural networks (Perozzi et al., 2014; Zhang et al., 2020). This direction was later surpassed by the message passing paradigm of GNNs (Gilmer et al., 2017), which became the dominant approach to learning graph representations. More recently, the success of sequence-native architectures such as the Transformer has renewed interest in serialization-based methods (Wang et al., 2024). Many existing graph-to-sequence pipelines are not reversible. Specifically, walk-based serializations break the graph into local fragments. Each sequence reflects only part of the graph, and even combining many walks cannot reconstruct the original structure or capture global connectivity (Xia et al., 2019). In another case, traversal-based serializations are sensitive to node ordering and starting choices, so even isomorphic graphs may produce different graph traversal circuit (Gao et al., 2025). In contrast, our method is reversible and almost invariant to graph permutation.

Tokenization The Transformer architecture has become the standard paradigm for sequence modeling (Vaswani et al., 2017). Its success is closely tied to the use of effective tokenization (Floridi & Chiriatti, 2020; Guo et al., 2025), which is especially critical in LLMs. A tokenizer converts raw input (e.g., text) into a sequence of discrete symbols, with BPE being a widely adopted data-driven approach that builds a vocabulary by iteratively merging frequent symbol pairs (Shibata et al., 1999). In prior work on graph data, the term *graph tokenization* has been used with different meanings. It has referred to neural encoders that produce continuous embeddings (Tang et al., 2024), pooling or coarsening modules that compress subgraphs into super-nodes (Shen & Póczos, 2024), and vector quantization components that discretize node features or latent representations (Yang et al., 2023). In this paper, we adopt the common sense in natural language processing, where a tokenizer is a

procedure that maps a labeled graph to a sequence of discrete symbols for direct use by sequence models.

3 METHOD

3.1 PRELIMINARIES

Graph. A graph is a tuple $G = (\mathcal{V}, \mathcal{E})$, composed of a finite set of nodes $\mathcal{V}$ and a set of edges $\mathcal{E}$. Our work focuses on *labeled graphs*, which we define as a tuple $\mathcal{G} = (G, L, \Sigma)$, where Σ is a finite alphabet of symbols and $L : \mathcal{V} \cup \mathcal{E} \to \Sigma$ is a labeling function. Two labeled graphs $\mathcal{G}_1 = (G_1, L_1, \Sigma)$ and $\mathcal{G}_2 = (G_2, L_2, \Sigma)$ are *isomorphic*, denoted $\mathcal{G}_1 \cong \mathcal{G}_2$, if there exists a graph isomorphism $\phi : \mathcal{V}_1 \to \mathcal{V}_2$ between G_1 and G_2 that also preserves all labels.

Graph Serialization. In general, a graph serialization function f maps a graph to a finite sequence of symbols. Let $\mathcal{A}$ denote the universe of possible sequence elements. The mapping is defined as

$$f : \mathcal{G} \mapsto (s_1, s_2, \ldots, s_k) \quad \text{s.t. } s_i \in \mathcal{A} \text{ for } 1 \leq i \leq k. \tag{1}$$

The choice of $\mathcal{A}$ depends on the serialization method. It may consist of node identifiers ($\mathcal{A} = \mathcal{V}$), continuous embeddings ($\mathcal{A} = \mathbb{R}^d$), or discrete labels ($\mathcal{A} = \mathbb{Z}$). For the purpose of building a discrete tokenizer, we focus on serializations where the output sequence is composed of symbols from the graph's alphabet, i.e., $\mathcal{A} = \Sigma$. To serve as a reliable interface, such a serialization should satisfy two key properties:

- **Reversibility.** A serialization f is reversible if the original labeled graph $\mathcal{G}$ can be recovered from its sequence $S = f(\mathcal{G})$ up to isomorphism. Formally, let $f^{-1}(S)$ denote the set of all graphs that could produce sequence S. The serialization is reversible if for any $\mathcal{G}$ in the domain of f, there exists a reversed graph $\mathcal{G}' \in f^{-1}(f(\mathcal{G}))$ such that $\mathcal{G}' \cong \mathcal{G}$.
- **Determinism.** A serialization function f is deterministic if, for any labeled graph $\mathcal{G}$, it consistently produces the same sequence S. This property is essential for addressing the permutation-invariance of graphs. A deterministic serialization generates a stable sequence for all graphs within an isomorphism class.

Graph Tokenization. A graph tokenizer Φ maps a labeled graph $\mathcal{G}$ to a finite sequence of discrete symbols, referred to as tokens.

$$\Phi : \ \mathcal{G} \ \mapsto \ S_{\mathrm{T}} = (t_1, \ldots, t_m), \quad t_j \in \mathcal{V}_T. \tag{2}$$

In this work, we construct the graph tokenizer Φ by composing a graph serialization function f with a sequence tokenizer T inspired by the text tokenizers used in LLMs. The sequence tokenizer T maps a sequence over the initial alphabet Σ to a new sequence over a target vocabulary $\mathcal{V}_T$, where the vocabulary is typically learned from data using BPE. The overall mapping is given by

$$\Phi = T \circ f. \tag{3}$$

When a decoding procedure is available, the original graph can be reconstructed up to isomorphism by applying the inverse operations T^{-1} followed by f^{-1}. Specifically, the term *graph tokenizer* refers to methods that produce a discrete sequence. Methods that only discretize embeddings (Yang et al., 2023) or apply pooling or coarsening (Shen & Póczos, 2024) are not considered tokenizers in this sense.

3.2 GRAPH TOKENIZER

We construct our graph tokenizer Φ by composing a reversible and structure-guided serialization function f with a tokenization step T based on BPE. To ensure graph structural information is preserved, f is designed to be *reversible*, and to produce stable sequences, we enforce a *deterministic* guiding policy for f. We propose a data-driven graph tokenizer Φ that is learned from a training corpus of graphs rather than relying on hand-crafted heuristics. Specifically, Algorithm 1 details the training, encoding, and decoding procedures of `GraphTokenizer`, and Figure 1 illustrates the overall framework.

Local Structural Pattern Statistics. The training procedure begins with the computation of dataset-level statistics of local patterns, which provide a data-driven basis for ensuring determinism in graph serialization. As illustrated in Fig. 1A, we count how often small labeled patterns appear in the training graphs, using molecular graphs and edge patterns as an example. These counts are then normalized into relative frequencies.

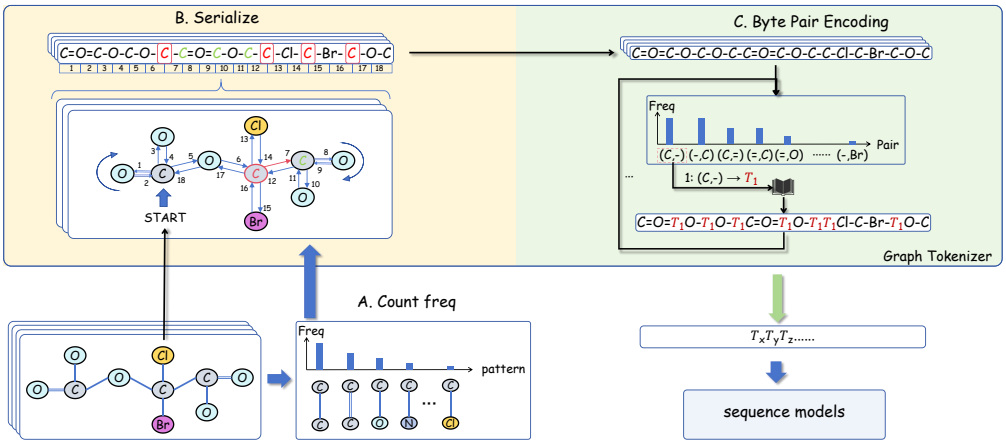

Figure 1: Framework of the proposed graph tokenizer. (A) Substructure frequencies are collected from the training graphs. (B) Structure-guided and reversible serialization is performed using a frequency-guided Eulerian circuit, where the next edge is selected according to a priority rule (e.g., red C: 7→13→15→17). (C) A BPE vocabulary is trained on the serialized corpus, and graphs are encoded into discrete tokens for use in downstream sequence models.

For a labeled graph $\mathcal{G} = ((\mathcal{V}, \mathcal{E}), L, \Sigma)$, we define a basic local pattern as a labeled edge $p = (l_u, l_e, l_v) \in \Sigma^3$, which captures the labels of the source node, the edge, and the target node. Intuitively, this is the smallest substructure that still reflects a typed relation between two labeled entities. Compared with larger subgraphs, it is computationally inexpensive, permutation-invariant over node indices, and stable under isomorphisms, which makes it a practical choice for tie-breaking during graph serialization. The count of p in $\mathcal{G}$ is given by

$$\mathrm{Count}(\mathcal{G}, p) = \big|\{\, e = (u, v) \in \mathcal{E} \;\mid\; (L(u), L(e), L(v)) = p \,\}\big|. \tag{4}$$

Aggregating over the training set $\mathcal{D}$, we obtain raw counts and their normalized relative frequencies as

$$C(p) = \sum_{\mathcal{G} \in \mathcal{D}} \mathrm{Count}(\mathcal{G}, p) \qquad F(p) = \frac{C(p)}{\sum_{p' \in \Sigma^3} C(p')}. \tag{5}$$

$F(p)$ denotes the normalized relative frequency, while raw counts $C(p)$ are introduced here as an intermediate definition.

Structure-Guided Reversible Serialization. We proceed to the next step of our framework, where each graph is converted into a sequence of symbols (Algorithm 1, **line 5**). In this procedure, line 4 corresponds to estimating F from data, and the resulting frequency map will guides the structure-aware serialization function $f_g(\cdot, F)$. The function f_g addresses traversal ambiguities by prioritizing edges whose incident labeled pattern has higher $F(p)$ from itself and neighbors, with fixed lexical rules applied to break any remaining ties.

Table 1: Properties of graph serialization methods. For Random Walk, L is walk length and R the number of walks. Implementation details are in Appendix B.

Method	Reversibility	Determinism	Time Complexity
Random Walk	No	No	$O(RL)$
Node-list BFS/DFS	No	No	$O(\lvert\mathcal{V}\rvert + \lvert\mathcal{E}\rvert)$
Topological Sort	No	No	$O(\lvert\mathcal{V}\rvert + \lvert\mathcal{E}\rvert)$
Eulerian circuit	Yes	No	$O(\lvert\mathcal{E}\rvert)$
SMILES (non-canonical)	Yes	No	$O(\lvert\mathcal{V}\rvert + \lvert\mathcal{E}\rvert)$
Canonical SMILES	Yes	Yes	$O(\lvert\mathcal{V}\rvert + \lvert\mathcal{E}\rvert)$
Chinese Postman Problem	Yes	No	$O(\lvert\mathcal{V}\rvert^3)$
Frequency-Guided Eulerian circuit	**Yes**	**Yes**	$\boldsymbol{O(\lvert\mathcal{E}\rvert)}$
Frequency-Guided CPP	**Yes**	**Yes**	$\boldsymbol{O(\lvert\mathcal{V}\rvert^3)}$

Fig. 1B illustrates this serialization process on a molecular graph. Specifically, at the red node C, the next step is chosen by the F-guided priority rather than arbitrarily(e.g., choose the green node C be-

cause "C-C" pair has the highest frequency). To ensure that graph serialization yields faithful graph representations, we require it to satisfy the properties of reversibility and determinism discussed in Section 3.1. Ensuring that these two properties hold simultaneously for general graphs is a significant challenge. To motivate our approach, we first review classical serialization methods against these criteria. To provide a clear overview, Table 1 summarizes the properties of existing serialization methods. A key limitation is that no classical method is simultaneously broadly applicable, fully reversible, and inherently deterministic.

Early approaches such as *Random Walks* (Perozzi et al., 2014) are inherently stochastic and typically explore only a local portion of the graph per sample. Even when many walks are aggregated, substructures are split across sequences without markers, so reconstruction is not guaranteed, and the procedure remains non-deterministic. Standard traversal algorithms like *Breadth-First Search (BFS)* (Moore, 1959) and *Depth-First Search (DFS)* (Even & Even, 2011) also fail to meet these requirements. Their non-determinism arises from arbitrary neighbor selection when multiple choices are available, and their node-list output omits edge connectivity, which prevents reconstruction of the original graph. *Topological Sort* (Kahn, 1962), which produces linear orderings for Directed Acyclic Graphs (DAGs), is limited to DAGs and admits multiple valid orderings, making it non-deterministic. Moreover, like other node-list traversals, it is not reversible because the precise edge connectivity information necessary for reconstruction is discarded.

Algorithm 1 The `GraphTokenizer` Framework

Procedure TRAIN($\mathcal{D}, K$)
Input: A training graph dataset $\mathcal{D}$; number of BPE merges K.
Output: frequency map F; BPE codebook $\mathcal{C} = (\mathcal{V}_T, \mathcal{R})$.
$F(p) \leftarrow \sum_{\mathcal{G}\in\mathcal{D}} \text{Count}(\mathcal{G}, p), \quad \forall p \in \Sigma^3$
$\mathcal{D}_S \leftarrow \{\, f_g(\mathcal{G}, F) \mid \mathcal{G} \in \mathcal{D} \,\}$
$\mathcal{V}_T \leftarrow \Sigma;\ \mathcal{R} \leftarrow \emptyset$
for $k = 1$ to K **do**
  $(s_a^*, s_b^*) \leftarrow \arg\max_{(s_a,s_b)} \sum_{S\in\mathcal{D}_S} \text{Count}(S, (s_a, s_b))$
  $s_{\text{new}} \leftarrow s_a^* \cdot s_b^*$
  $\mathcal{V}_T \leftarrow \mathcal{V}_T \cup \{s_{\text{new}}\}$
  $\mathcal{R} \leftarrow \mathcal{R} \cup \{(s_a^*, s_b^*) \rightarrow s_{\text{new}}\}$
  for each $S \in \mathcal{D}_S$ **do**
    replace all disjoint adjacent pairs (s_a^*, s_b^*) in S with s_{new}
return $(F, \mathcal{C})$

Procedure ENCODE($\mathcal{G}, F, \mathcal{C}$)
Input: graph $\mathcal{G}$; frequency map F; the codebook $\mathcal{C} = (\mathcal{V}_T, \mathcal{R})$.
Output: A token sequence S_T.
$S \leftarrow f_g(\mathcal{G}, F)$
for each $(s_a, s_b) \rightarrow s_{\text{new}}$ in $\mathcal{R}$ **do**
  replace all disjoint adjacent pairs (s_a, s_b) in S with s_{new}
$S_T \leftarrow S$
return S_T

Procedure DECODE($S_T, \mathcal{C}, f^{-1}$)
Input: token sequence S_T; codebook $\mathcal{C} = (\mathcal{V}_T, \mathcal{R})$; inverse serialization function f^{-1}.
Output: A reconstructed graph $\widehat{\mathcal{G}}$.
$S \leftarrow S_T$
for each $(s_a, s_b) \rightarrow s_{\text{new}}$ in reversed($\mathcal{R}$) **do**
  replace every s_{new} in S with the pair (s_a, s_b)
$\widehat{\mathcal{G}} \leftarrow f^{-1}(S)$
return $\widehat{\mathcal{G}}$

In contrast to node-based traversals, methods that cover every edge of the graph are naturally reversible. A representative example is the *Eulerian circuit* (Biggs et al., 1986), which visits each edge exactly once. By treating each undirected edge as two opposing directed edges, the method can extend to any connected graph (Gao et al., 2025). During traversal, emitting an alternating *node–edge–node* sequence ensures that adjacent symbols share an endpoint, which preserves the

information needed by f^{-1} to reconstruct the edges. Despite this reversibility, the method remains non-deterministic because the classical Hierholzer's algorithm (Hierholzer & Wiener, 1873) must make arbitrary choices whenever a node has multiple unvisited edges. A related approach is the *Chinese Postman Problem (CPP)* (Kwan, 1960), which seeks a minimum weight traversal that covers all edges and thereby also preserves the complete graph structure. Non-determinism in CPP, although more constrained, is intrinsic to its solution process, typically solved using Edmonds' blossom algorithm (Edmonds & Johnson, 1973). The standard procedure first identifies all odd-degree nodes and constructs an auxiliary complete graph on them, with edge weights representing shortest path distances in the original graph. A minimum-weight perfect matching is then computed to determine which paths should be duplicated. If multiple minimum-weight matchings exist, the selection between them is arbitrary, which dictates the different possible traversals.

Domain-specific serialization methods for molecular graphs, such as SMILES (Weininger, 1988), represent a widely adopted approach in cheminformatics. Non-canonical SMILES is reversible but not deterministic, whereas canonical SMILES achieves determinism by applying an explicit canonicalization procedure under a fixed scheme. These procedures rely on chemistry-specific perception rules (e.g., aromaticity, implicit hydrogens, and structural notations) and therefore do not generalize to arbitrary labeled graphs. Furthermore, the determinism of canonical SMILES is defined relative to the chosen canonicalization algorithm and perception rules, and implementations may differ slightly across toolkits.

Building on the preceding analysis, our strategy is to impose determinism on traversal methods that are inherently reversible. This is accomplished by introducing a guiding mechanism that leverages the global frequency map F to resolve traversal ambiguities. In this way, we obtain a structure-guided graph serialization function f_g that simultaneously satisfies reversibility and determinism for general graphs.

Frequency-Guided Eulerian circuit adapts Hierholzer's algorithm by introducing a priority rule. At any node u with unvisited outgoing edges $\mathcal{E}_u$, the next edge e^* is selected deterministically as

$$e^* = \arg\max_{e_i \in \mathcal{E}_u} \pi(e_i, F), \tag{6}$$

where $\pi(e_i, F)$ assigns a scalar priority, for example $\pi(e_i, F) = F(p_i)$ for the pattern $p_i = (L(u), L(e_i), L(v))$. Although traversal may begin from any node, the resulting circuit differs only by a cyclic shift.

For example, in Fig. 1B, when the traversal reaches the red C, there are four candidate neighbors (including the incoming one). According to the dataset-level statistics F, the C–C labeled-edge pattern has the highest $F(p)$, so f_g takes that step (step 3). When it later returns to the same red C, it selects among the remaining three neighbors: the edge to Cl has the next-highest $F(p)$ (step 5), followed by steps 7 and 9.

Frequency-Guided CPP incorporates frequency statistics into the edge weights used by the solver. For an edge e with associated pattern p_e, the weight is defined as

$$w(e) = \alpha \cdot 1 + (1 - \alpha) \cdot g(F(p_e)), \tag{7}$$

where g is a decreasing function of frequency (e.g., $1/F(p_e)$) and $\alpha \in [0, 1]$ is a tunable hyperparameter. Ties that arise during matching or tour construction are resolved using the priority policy specified in Eq. 6. For disconnected graphs, each component is serialized independently and the results are concatenated in a fixed order.

Vocabulary Learning via BPE. After converting the graph dataset $\mathcal{D}$ into a corpus of symbol sequences $\mathcal{D}_S$, the final stage of training is to learn a vocabulary from this corpus. We employ Byte Pair Encoding (BPE), inspired by the text tokenizers used in LLMs, corresponding to the main loop in Algorithm 1 (**lines 6–14**). BPE iteratively identifies the most frequently occurring adjacent pair of symbols in the corpus and merges it into a new symbol added to the vocabulary. Fig. 1C illustrates the vocabulary learning procedure on a serialized molecular sequence. In this example, a pair denotes an adjacent atom–bond symbol, e.g. $(\mathrm{C}, -)$. At each iteration i, the most frequent pair is replaced at all disjoint occurrences by a new token T_i, and the corresponding merge rule $(s_a, s_b) \to T_i$ is added to the codebook $\mathcal{C}$. The updated sequence is then passed back to the counting step, forming an iterative training loop.

The key insight of our framework lies in the interplay between structure-guided serialization and the BPE algorithm. The serialization function f_g is not merely a format conversion tool but leverages the

global frequency map F to ensure that statistically common local graph structures are systematically encoded as frequently adjacent symbol pairs in the sequence corpus $\mathcal{D}_S$. This structured corpus forms an ideal input for BPE's greedy merging strategy. When BPE merges the most frequent pair (s_a^*, s_b^*) (**line 8**), the operation is not arbitrary compression but the discovery of statistically salient tokens derived from graph data. Each merged token represents a larger subgraph fragment that can be recovered from the serialization. The resulting vocabulary $\mathcal{V}_T$ provides a data-driven, structurally informed representation of the graph for the downstream Transformer.

Encoding and Decoding. After training, the procedure produces two components for inference: the frequency map F and the BPE codebook $\mathcal{C}$. To encode a new graph, the ENCODE procedure in Algorithm 1 is applied. The graph is first serialized into a symbol sequence by the function f, we apply the merge rules $\mathcal{R}$ from $\mathcal{C}$ in the learned order to obtain the final token sequence S_T. The DECODE procedure in Algorithm 1 reverses this process. The tokens in S_T are first expanded back into the original symbol sequence by applying the inverse of $\mathcal{R}$, and the inverse serialization function f^{-1} then reconstructs the graph. These procedures ensure that the mapping between graphs and sequences is both reversible and deterministic, providing a bidirectional interface between the two domains.

Applications. The primary output of our framework is a discrete sequence of tokens S_T that faithfully encodes the original graph. This sequential representation provides an interface through which the Transformer ecosystem can be directly applied to graph-structured data (Vaswani et al., 2017). For graph-level prediction tasks such as classification or regression, the token sequence can be processed by an encoder-only model (e.g., BERT). A special `[CLS]` token may be prepended, or the final hidden states pooled, to derive a vector representation for the entire graph (Perozzi et al., 2014). For generative tasks, a decoder-only model (e.g., GPT) can be trained to generate graphs autoregressively by predicting the next token in the sequence, supporting applications such as molecular or material discovery (Radford et al., 2019). Multimodal models can also support tasks such as graph summarization, where we use pretrained graph representations from the proposed tokenizer with a large language model to generate concise descriptions of input graphs (Yamagata et al., 2023).

In summary, the proposed graph tokenizer reframes graph representation learning as a sequence modeling problem. Our method decouples the structural complexity of graphs from the architectural design of the model and enables direct use of advances in sequence modeling, such as longer context windows (Ding et al., 2022) and more efficient attention mechanisms (Dao et al., 2022) for a wide range of graph learning tasks.

4 EXPERIMENTS

In this section, we evaluate our proposed graph tokenizer, `GraphTokenizer` (GT). We aim to answer the following questions: (1) How effectively does BPE compress the serialized graph representations, and what is the efficiency of our approach in terms of sequence length, processing speed, and training throughput? (2) How does our framework, when paired with standard Transformer models, perform against state-of-the-art graph representation learning methods? (3) How do different design choices, such as the serialization method and BPE usage, affect performance? (4) Can the learned vocabulary and model attention provide interpretable insights into graph structures?

4.1 EXPERIMENTAL SETUP

Datasets. We evaluate our method on 14 diverse public datasets for graph classification and regression. The benchmarks span multiple domains, including molecular graphs such as Mutagenicity (`Muta`) and Proteins (Riesen & Bunke, 2008), OGBG-molhiv (Hu et al., 2020), ZINC (Irwin et al., 2012), AQSOL (Sorkun et al., 2019),and QM9 (Wu et al., 2018); computer vision graphs like COIL-DEL (Rossi & Ahmed, 2015); graph theory like Colors-3 (Knyazev et al., 2019) and Synthetic (Feragen et al., 2013); biomedical graphs like DD (Dobson & Doig, 2003) (Bechler-Speicher et al., 2024) and Peptides (Freitas et al., 2020); social networks (Twitter (Pan et al., 2015)); and academic networks (DBLP (Pan et al., 2013)). A summary of dataset statistics is provided in Appendix C.1.

Baselines. Our approach is benchmarked against a comprehensive set of baselines, ranging from classic GNNs (GCN (Kipf, 2016), GIN (Chen et al., 2019)) to state-of-the-art models, including the powerful GCN+ (Luo et al., 2025), Graph Transformers like GraphGPS (Rampášek et al., 2022), and the serialization-based GraphMamba (Wang et al., 2024). To ensure a fair comparison, all baseline results are from official implementations run on our unified data splits and preprocessing pipeline (Dwivedi et al., 2023; Luo et al., 2025; 2023; Bechler-Speicher et al., 2024). Results on key benchmarks are in the main text; the rest are in Appendix D. The baseline results in our main tables

are primarily obtained by running the official or widely used open-source implementations on our unified data splits and preprocessing pipeline, ensuring a fair comparison (Dwivedi et al., 2023; Luo et al., 2025; 2023; Bechler-Speicher et al., 2024).Results on widely used standard benchmarks are included in the main text, and results on the remaining datasets are provided in Appendix D.

Implementation Details. Our proposed method, `GraphTokenizer` (GT), encodes graphs into token sequences that are subsequently processed by a standard Transformer model for downstream tasks. We report results with two Transformer backbones: (1) **GT+BERT**, which adopts the BERT-small architecture (Devlin et al., 2019), and (2) **GT+GTE**, which uses the more recent GTE model with a parameter count comparable to BERT-base (Zhang et al., 2024). Unless otherwise specified, the tokenizer applies the Frequency-Guided Eulerian circuit (`Feuler`) serialization method followed by Byte Pair Encoding (BPE) on the resulting sequences. Further details on model architectures, dataset splits, and hyperparameter settings are provided in Appendix C.3.

4.2 Performance Results

We present the main performance comparison on a representative subset of classification and regression benchmarks in Tables 2. For each dataset, we report the mean and standard deviation of the primary evaluation metric on five independent runs.

Sequence length and efficiency. Figure 2 illustrates the impact of our tokenizer on efficiency. As shown in Figure 2a, BPE achieves a high compression ratio, reducing sequence lengths from reversible methods to approximately 10% of their original size. Notably, the frequency-guided Eulerian method (`Feuler`) produces more compact sequences post-BPE than its unguided counterpart, confirming that our structure-guided serialization is particularly well-suited for BPE. This compression translates directly to improved training efficiency. Figure 2b shows that with BPE, our approach using a standard Transformer backbone becomes significantly more efficient than specialized Graph Transformers like GraphGPS and even surpasses classic GNNs such as GatedGCN. While the speedup (e.g., $\sim$2.5$\times$ on `zinc` for a 10$\times$ compression) is not linear due to model overhead, the gains are substantial. This demonstrates that our graph tokenization framework not only enables standard sequence models to process graphs but also makes them a highly efficient and performant option for graph learning tasks.

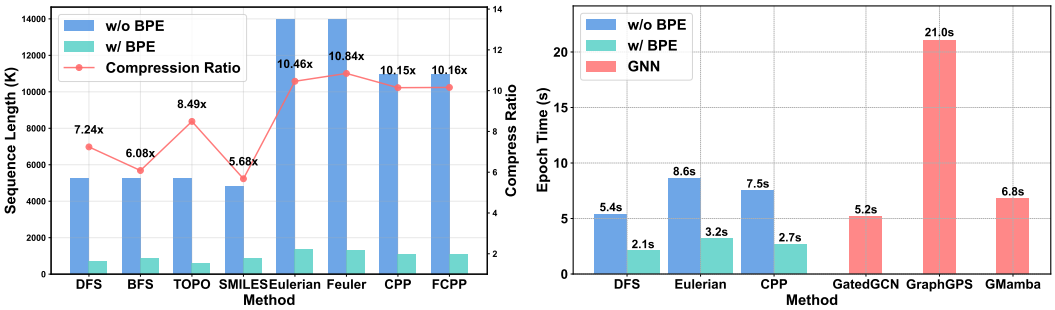

(a) BPE achieves high compression ratios.

(b) Training time per epoch.

Figure 2: Efficiency analysis on the ZINC dataset. (a) BPE greatly reduces token sequence length from serialization. (b) Graph tokenization leads to substantial training speedup by enabling efficient processing with standard Transformers.

Classification and Regression. Table 2 presents the performance on classification and regression benchmarks, reporting the mean and standard deviation over five independent runs. Our approach, particularly with the GTE backbone (GT+GTE), achieves state-of-the-art results on a majority of the 14 benchmarks. On the `ogbg-molhiv` benchmark, for instance, GT+GTE attains an ROC-AUC of 0.876 on our test split (val 0.903), significantly exceeding reported leaderboard results (test 0.8475, val 0.8275). This strong performance is achieved using an off-the-shelf sequence model without any graph-specific architectural modifications. Furthermore, the framework's effectiveness is evident even with the compact GT+BERT model, which already outperforms strong baselines on several datasets. Critically, scaling up to the larger GT+GTE backbone yields consistent performance gains across the board, demonstrating a clear advantage over many GNN architectures that can suffer from performance degradation with increased model capacity due to issues like over-smoothing.

4.3 Ablation Studies

We conduct ablation studies to evaluate the impact of different serialization methods and the BPE tokenization step while keeping the GT+GTE backbone fixed. Table 3 shows that the choice of

Table 2: Results of classification (left block) and regression (right block). The best scores are shown in bold, the second-best are underlined, and standard deviations are given in parentheses. Results for the remaining datasets are presented in Appendix D.

Model	molhiv auc↑	p-func ap↑	mutag acc↑	coildel acc↑	dblp acc↑	qm9 mae↓	zinc mae↓	aqsol mae↓	p-struct avg mae↓
GCN	74.0 (0.9)	53.2 (1.4)	79.7 (1.7)	74.6 (0.4)	76.6 (0.8)	0.134 (0.004)	0.399 (0.006)	1.345 (0.013)	0.342 (0.003)
GIN	76.1 (1.1)	61.4 (0.7)	80.4 (1.2)	72.0 (0.8)	73.8 (0.9)	0.176 (0.006)	0.379 (0.007)	2.053 (0.058)	0.338 (0.002)
GAT	72.1 (0.8)	51.2 (1.1)	80.1 (0.9)	74.4 (1.1)	76.3 (0.7)	0.114 (0.015)	0.445 (0.015)	1.388 (0.008)	0.316 (0.003)
GatedGCN	80.6 (0.6)	51.2 (1.0)	83.6 (0.8)	83.7 (0.4)	86.0 (0.4)	0.096 (0.007)	0.370 (0.011)	0.940 (0.016)	0.312 (0.004)
GraphGPS	78.5 (1.5)	53.5 (0.7)	84.3 (0.9)	80.5 (0.8)	71.6 (0.8)	0.084 (0.004)	0.310 (0.005)	1.587 (0.011)	0.251 (0.001)
Exphormer	82.3 (0.7)	64.5 (0.9)	82.7 (1.1)	**91.5** (0.2)	84.9 (0.8)	0.080 (0.005)	0.281 (0.006)	0.749 (0.006)	0.251 (0.002)
GraphMamba	81.2 (0.5)	67.7 (0.9)	85.0 (1.0)	74.5 (1.1)	87.6 (0.5)	0.083 (0.005)	0.209 (0.009)	1.133 (0.014)	0.248 (0.002)
GCN+	80.1 (0.6)	72.6 (0.6)	88.7 (0.6)	88.9 (0.3)	89.6 (0.4)	0.077 (0.003)	**0.116** (0.009)	0.712 (0.009)	0.244 (0.001)
GT+BERT	82.6 (0.4)	68.5 (0.5)	87.5 (0.9)	74.1 (0.4)	93.2 (0.1)	0.122 (0.008)	0.241 (0.011)	0.648 (0.008)	0.247 (0.002)
GT+GTE	**87.4** (0.2)	**73.1** (0.2)	**90.1** (0.7)	89.6 (0.2)	**93.6** (0.1)	**0.071** (0.004)	0.131 (0.007)	**0.609** (0.016)	**0.242** (0.001)

serialization has a significant impact on performance. Reversible methods that traverse every edge (e.g., Eulerian and CPP variants) significantly outperform non-reversible node-list traversals, with only a few exceptions detailed in Appendix D. Within the reversible category, the frequency-guided Eulerian circuit (`Feuler`) demonstrates a clear advantage over its unguided counterpart, not only in mean performance but also in reduced variance, indicating greater stability. In contrast, the performance gap between CPP and its frequency-guided version (`FCPP`) remains minimal. A plausible explanation is that CPP's objective of finding a minimum-weight traversal already yields a highly structured sequence, leaving limited room for further improvement from frequency-based guidance. Although `FCPP` performs comparably to `Feuler`, `Feuler` provides substantial benefits in algorithmic complexity (Appendix B.4) and scalability, making it more practical choice for larger graphs.

A second key finding is that applying BPE to serialized sequences substantially improves model performance. Across nearly all configurations, BPE yields higher scores with a clear performance margin. This improvement is accompanied by reduced standard deviation, indicating more stable and reliable training. Moreover, these performance gains come in addition to the substantial efficiency improvements discussed previously in Figure 2. Therefore, BPE is a critical component of our framework, enhancing both accuracy and computational efficiency.

Table 3: Ablation of serialization method orderings with and without BPE. The best scores are shown in bold, the second-best are underlined, and standard deviations are given in parentheses. A dash ("—") under the SMILES method indicates that the dataset either lacks SMILES representations or does not correspond to a molecular graph.

Method	molhiv auc↑		coildel acc↑		p-func ap↑		zinc mae↓		qm9 mae↓	
	w	w/o	w	w/o	w	w/o	w	w/o	w	w/o
BFS	72.3 (0.6)	81.2 (0.9)	81.2 (0.9)	80.1 (1.3)	68.5 (0.6)	67.2 (0.2)	0.453 (0.011)	0.696 (0.013)	0.311 (0.009)	0.292 (0.011)
DFS	76.0 (0.4)	79.1 (0.5)	80.5 (0.4)	79.8 (0.8)	71.0 (1.1)	68.4 (0.3)	0.446 (0.009)	0.705 (0.008)	0.291 (0.007)	0.277 (0.010)
TOPO	73.2 (0.6)	75.6 (0.8)	82.6 (0.8)	81.4 (1.2)	67.9 (0.3)	64.5 (0.5)	0.416 (0.010)	0.634 (0.011)	0.293 (0.010)	0.275 (0.013)
Eulerian	84.5 (0.7)	81.0 (1.0)	84.1 (1.5)	84.0 (1.5)	69.1 (0.6)	66.8 (1.1)	0.164 (0.009)	0.160 (0.016)	0.083 (0.004)	0.104 (0.008)
Feuler	**87.4** (0.4)	81.3 (0.5)	88.0 (0.7)	85.6 (0.6)	**73.1** (0.3)	68.1 (0.9)	**0.131** (0.007)	0.171 (0.013)	**0.071** (0.005)	0.088 (0.007)
CPP	86.9 (0.3)	81.2 (0.5)	**89.6** (0.1)	86.7 (0.3)	69.2 (0.2)	67.0 (0.8)	0.141 (0.006)	0.145 (0.009)	0.073 (0.004)	0.093 (0.006)
FCPP	86.4 (0.3)	81.0 (0.6)	89.4 (0.3)	86.8 (1.0)	69.2 (0.3)	66.3 (0.5)	0.140 (0.005)	0.151 (0.008)	0.079 (0.005)	0.095 (0.007)
SMILES	—	—	—	—	—	—	0.201 (0.012)	0.339 (0.009)	0.092 (0.008)	0.081 (0.014)

5 Conclusion

In this paper, we introduce a general framework for graph tokenization that bridges graph-structured data with the Transformer ecosystem. Our approach combines reversible, structure-guided graph serialization with BPE to construct a faithful and efficient interface that encodes graphs into discrete token sequences. Fundamentally, the framework decouples the design of graph representations from the underlying model architecture, thereby reframing graph learning as a sequence modeling problem. This perspective enables graph data to be directly integrated into general-purpose Transformers, allowing the graph learning field to leverage rapid advancements in model architectures, training strategies, and scaling capabilities. Empirically, we demonstrate that this approach enables standard off-the-shelf Transformers to process graph data effectively and achieve state-of-the-art results on a diverse set of benchmarks, outperforming established GNNs and specialized Graph Transformers. Limitations of this work and directions for future research are discussed in Appendix A.

Ethics Statement

The authors of this work have read and commit to adhering to the Code of Ethics. Our research proposes a foundational framework for graph tokenization and, to the best of our knowledge, does not present any direct ethical concerns. The work does not involve the use of personally identifiable information, sensitive human-subject data, or applications with immediate potential for societal harm.

Reproducibility Statement

To ensure full reproducibility, our complete source code is provided in the supplementary materials. This source code contains training configuration files for all experiments, and the necessary scripts to preprocess datasets from their original sources. For convenience, ready-to-use versions of the datasets are also provided. Comprehensive details on the experimental setup are documented in the Appendix, including the datasets (Appendix C.1), model architectures (Appendix C.2), hyperparameter configuration (Appendix C.3), and runtime environment (Appendix C.4).

References

Maya Bechler-Speicher, Amir Globerson, and Ran Gilad-Bachrach. The intelligible and effective graph neural additive network. *Advances in Neural Information Processing Systems*, 37:90552–90578, 2024.

N. Biggs, E.K. Lloyd, and R.J. Wilson. *Graph Theory, 1736-1936*. Clarendon Press, 1986. ISBN 9780198539162. URL https://books.google.pn/books?id=XqYTk0sXmpoC.

Runjin Chen, Tong Zhao, Ajay Jaiswal, Neil Shah, and Zhangyang Wang. Llaga: Large language and graph assistant. *arXiv preprint arXiv:2402.08170*, 2024.

Zhengdao Chen, Soledad Villar, Lei Chen, and Joan Bruna. On the equivalence between graph isomorphism testing and function approximation with gnns. *Advances in neural information processing systems*, 32, 2019.

Tri Dao, Dan Fu, Stefano Ermon, Atri Rudra, and Christopher Ré. Flashattention: Fast and memory-efficient exact attention with io-awareness. *Advances in neural information processing systems*, 35:16344–16359, 2022.

Jacob Devlin, Ming-Wei Chang, Kenton Lee, and Kristina Toutanova. Bert: Pre-training of deep bidirectional transformers for language understanding. In *Proceedings of the 2019 conference of the North American chapter of the association for computational linguistics: human language technologies, volume 1 (long and short papers)*, pp. 4171–4186, 2019.

Lei Ding, Dong Lin, Shaofu Lin, Jing Zhang, Xiaojie Cui, Yuebin Wang, Hao Tang, and Lorenzo Bruzzone. Looking outside the window: Wide-context transformer for the semantic segmentation of high-resolution remote sensing images. *IEEE Transactions on Geoscience and Remote Sensing*, 60:1–13, 2022.

Paul D Dobson and Andrew J Doig. Distinguishing enzyme structures from non-enzymes without alignments. *Journal of molecular biology*, 330(4):771–783, 2003.

Alexey Dosovitskiy, Lucas Beyer, Alexander Kolesnikov, Dirk Weissenborn, Xiaohua Zhai, Thomas Unterthiner, Mostafa Dehghani, Matthias Minderer, Georg Heigold, Sylvain Gelly, et al. An image is worth 16x16 words: Transformers for image recognition at scale. *arXiv preprint arXiv:2010.11929*, 2020.

Vijay Prakash Dwivedi, Chaitanya K Joshi, Anh Tuan Luu, Thomas Laurent, Yoshua Bengio, and Xavier Bresson. Benchmarking graph neural networks. *Journal of Machine Learning Research*, 24(43):1–48, 2023.

Jack Edmonds and Ellis L. Johnson. Matching, euler tours and the chinese postman. *Mathematical Programming*, 5:88–124, 1973. URL https://api.semanticscholar.org/CorpusID:15249924.

S. Even and G. Even. *Graph Algorithms*. Cambridge University Press, 2011. ISBN 9781139504157. URL https://books.google.com/books?id=m3QTSMYm5rkC.

Aasa Feragen, Niklas Kasenburg, Jens Petersen, Marleen De Bruijne, and Karsten Borgwardt. Scalable kernels for graphs with continuous attributes. *Advances in neural information processing systems*, 26, 2013.

Luciano Floridi and Massimo Chiriatti. Gpt-3: Its nature, scope, limits, and consequences. *Minds and machines*, 30(4):681–694, 2020.

Scott Freitas, Yuxiao Dong, Joshua Neil, and Duen Horng Chau. A large-scale database for graph representation learning. *arXiv preprint arXiv:2011.07682*, 2020.

Jian Gao, Weidong Cao, Junyi Yang, and Xuan Zhang. Analoggenie: A generative engine for automatic discovery of analog circuit topologies. *The Thirteenth International Conference on Learning Representations*, 2025.

Justin Gilmer, Samuel S Schoenholz, Patrick F Riley, Oriol Vinyals, and George E Dahl. Neural message passing for quantum chemistry. In *International conference on machine learning*, pp. 1263–1272. Pmlr, 2017.

Yuan Gong, Yu-An Chung, and James Glass. Ast: Audio spectrogram transformer. *arXiv preprint arXiv:2104.01778*, 2021.

Daya Guo, Dejian Yang, Haowei Zhang, Junxiao Song, Ruoyu Zhang, Runxin Xu, Qihao Zhu, Shirong Ma, Peiyi Wang, Xiao Bi, et al. Deepseek-r1: Incentivizing reasoning capability in llms via reinforcement learning. *arXiv preprint arXiv:2501.12948*, 2025.

Xiaoxin He, Bryan Hooi, Thomas Laurent, Adam Perold, Yann LeCun, and Xavier Bresson. A generalization of vit/mlp-mixer to graphs. In *International conference on machine learning*, pp. 12724–12745. PMLR, 2023.

Carl Hierholzer and Chr Wiener. Ueber die Möglichkeit, einen Linienzug ohne Wiederholung und ohne Unterbrechung zu umfahren. *Mathematische Annalen*, 6(1):30–32, March 1873. ISSN 1432-1807. doi: 10.1007/BF01442866. URL https://doi.org/10.1007/BF01442866.

Weihua Hu, Matthias Fey, Marinka Zitnik, Yuxiao Dong, Hongyu Ren, Bowen Liu, Michele Catasta, and Jure Leskovec. Open graph benchmark: Datasets for machine learning on graphs. *Advances in neural information processing systems*, 33:22118–22133, 2020.

John J Irwin, Teague Sterling, Michael M Mysinger, Erin S Bolstad, and Ryan G Coleman. Zinc: a free tool to discover chemistry for biology. *Journal of chemical information and modeling*, 52 (7):1757–1768, 2012.

A. B. Kahn. Topological sorting of large networks. *Commun. ACM*, 5(11):558–562, November 1962. ISSN 0001-0782. doi: 10.1145/368996.369025. URL https://doi.org/10.1145/368996.369025.

TN Kipf. Semi-supervised classification with graph convolutional networks. *arXiv preprint arXiv:1609.02907*, 2016.

Boris Knyazev, Graham W Taylor, and Mohamed Amer. Understanding attention and generalization in graph neural networks. *Advances in neural information processing systems*, 32, 2019.

Mei-ko Kwan. Graphic programming using odd or even points. *Acta Mathematica Sinica*, 10:263–266, 1960. Also translated in Chinese Mathematics 1, American Mathematical Society, 1962, pp. 273-277.

Xiao Luo, Yusheng Zhao, Zhengyang Mao, Yifang Qin, Wei Ju, Ming Zhang, and Yizhou Sun. Rignn: A rationale perspective for semi-supervised open-world graph classification. *Transactions on Machine Learning Research*, 2023.

Yuankai Luo, Lei Shi, and Xiao-Ming Wu. Can classic gnns be strong baselines for graph-level tasks? simple architectures meet excellence. *arXiv preprint arXiv:2502.09263*, 2025.

Shervin Minaee, Tomas Mikolov, Narjes Nikzad, Meysam Chenaghlu, Richard Socher, Xavier Amatriain, and Jianfeng Gao. Large language models: A survey. *arXiv preprint arXiv:2402.06196*, 2024.

E. F. Moore. The shortest path through a maze. In *Proc. International Symposium on the Theory of Switching, Part II*. harvard, 1959.

Shirui Pan, Xingquan Zhu, Chengqi Zhang, and Philip S Yu. Graph stream classification using labeled and unlabeled graphs. In *2013 IEEE 29th International Conference on Data Engineering (ICDE)*, pp. 398–409. IEEE, 2013.

Shirui Pan, Jia Wu, and Xingquan Zhu. Cogboost: Boosting for fast cost-sensitive graph classification. *IEEE Transactions on Knowledge and Data Engineering*, 27(11):2933–2946, 2015.

Bryan Perozzi, Rami Al-Rfou, and Steven Skiena. Deepwalk: Online learning of social representations. In *Proceedings of the 20th ACM SIGKDD international conference on Knowledge discovery and data mining*, pp. 701–710, 2014.

Alec Radford, Jeffrey Wu, Rewon Child, David Luan, Dario Amodei, Ilya Sutskever, et al. Language models are unsupervised multitask learners. *OpenAI blog*, 1(8):9, 2019.

Ladislav Rampášek, Michael Galkin, Vijay Prakash Dwivedi, Anh Tuan Luu, Guy Wolf, and Dominique Beaini. Recipe for a general, powerful, scalable graph transformer. *Advances in Neural Information Processing Systems*, 35:14501–14515, 2022.

Kaspar Riesen and Horst Bunke. Iam graph database repository for graph based pattern recognition and machine learning. In *Joint IAPR international workshops on statistical techniques in pattern recognition (SPR) and structural and syntactic pattern recognition (SSPR)*, pp. 287–297. Springer, 2008.

Ryan A. Rossi and Nesreen K. Ahmed. The network data repository with interactive graph analytics and visualization. In *AAAI*, 2015. URL `https://networkrepository.com`.

Yuchen Shen and Barnabás Póczos. Graphbpe: Molecular graphs meet byte-pair encoding. *arXiv preprint arXiv:2407.19039*, 2024.

Yusuxke Shibata, Takuya Kida, Shuichi Fukamachi, Masayuki Takeda, Ayumi Shinohara, Takeshi Shinohara, and Setsuo Arikawa. Byte pair encoding: A text compression scheme that accelerates pattern matching. *Technical Report DOI-TR-161, Department of Informatics, Kyushu University*, 1999.

Murat Cihan Sorkun, Abhishek Khetan, and Süleyman Er. Aqsoldb, a curated reference set of aqueous solubility and 2d descriptors for a diverse set of compounds. *Scientific data*, 6(1):143, 2019.

Jiabin Tang, Yuhao Yang, Wei Wei, Lei Shi, Lixin Su, Suqi Cheng, Dawei Yin, and Chao Huang. Graphgpt: Graph instruction tuning for large language models. In *Proceedings of the 47th International ACM SIGIR Conference on Research and Development in Information Retrieval*, pp. 491–500, 2024.

Ashish Vaswani, Noam Shazeer, Niki Parmar, Jakob Uszkoreit, Llion Jones, Aidan N Gomez, Łukasz Kaiser, and Illia Polosukhin. Attention is all you need. *Advances in neural information processing systems*, 30, 2017.

Chloe Wang, Oleksii Tsepa, Jun Ma, and Bo Wang. Graph-mamba: Towards long-range graph sequence modeling with selective state spaces. *arXiv preprint arXiv:2402.00789*, 2024.

David Weininger. Smiles, a chemical language and information system. 1. introduction to methodology and encoding rules. *Journal of chemical information and computer sciences*, 28(1):31–36, 1988.

Qitian Wu, Wentao Zhao, Chenxiao Yang, Hengrui Zhang, Fan Nie, Haitian Jiang, Yatao Bian, and Junchi Yan. Sgformer: Simplifying and empowering transformers for large-graph representations. *Advances in Neural Information Processing Systems*, 36:64753–64773, 2023.

Zhenqin Wu, Bharath Ramsundar, Evan N Feinberg, Joseph Gomes, Caleb Geniesse, Aneesh S Pappu, Karl Leswing, and Vijay Pande. Moleculenet: a benchmark for molecular machine learning. *Chemical science*, 9(2):513–530, 2018.

Feng Xia, Jiaying Liu, Hansong Nie, Yonghao Fu, Liangtian Wan, and Xiangjie Kong. Random walks: A review of algorithms and applications. *IEEE Transactions on Emerging Topics in Computational Intelligence*, 4(2):95–107, 2019.

Taku Yamagata, Ahmed Khalil, and Raul Santos-Rodriguez. Q-learning decision transformer: Leveraging dynamic programming for conditional sequence modelling in offline rl. In *International Conference on Machine Learning*, pp. 38989–39007. PMLR, 2023.

Ling Yang, Ye Tian, Minkai Xu, Zhongyi Liu, Shenda Hong, Wei Qu, Wentao Zhang, Bin Cui, Muhan Zhang, and Jure Leskovec. Vqgraph: Rethinking graph representation space for bridging gnns and mlps. *arXiv preprint arXiv:2308.02117*, 2023.

Shuo Yu, Yingbo Wang, Ruolin Li, Guchun Liu, Yanming Shen, Shaoxiong Ji, Bowen Li, Fengling Han, Xiuzhen Zhang, and Feng Xia. Graph2text or graph2token: A perspective of large language models for graph learning. *arXiv preprint arXiv:2501.01124*, 2025.

Seongjun Yun, Minbyul Jeong, Raehyun Kim, Jaewoo Kang, and Hyunwoo J Kim. Graph transformer networks. *Advances in neural information processing systems*, 32, 2019.

Jiawei Zhang, Haopeng Zhang, Congying Xia, and Li Sun. Graph-bert: Only attention is needed for learning graph representations. *arXiv preprint arXiv:2001.05140*, 2020.

Shuaicheng Zhang, Haohui Wang, Si Zhang, and Dawei Zhou. Gpatcher: A simple and adaptive mlp model for alleviating graph heterophily. *arXiv preprint arXiv:2306.14340*, 2023.

Xin Zhang, Yanzhao Zhang, Dingkun Long, Wen Xie, Ziqi Dai, Jialong Tang, Huan Lin, Baosong Yang, Pengjun Xie, Fei Huang, et al. mgte: Generalized long-context text representation and reranking models for multilingual text retrieval. In *Proceedings of the 2024 Conference on Empirical Methods in Natural Language Processing: Industry Track*, pp. 1393–1412, 2024.

Appendix

A Discussion

This section provides a candid discussion of our framework's limitations and outlines promising avenues for future research.

A.1 Limitations

Graphs with Continuous Features. Our framework operates by first converting a labeled graph into a sequence of discrete symbols, which subsequently forms the input for Byte Pair Encoding (BPE). This process implicitly assumes that the features associated with nodes and edges are discrete and can be directly mapped to an initial symbol alphabet. Consequently, graphs where attributes are primarily continuous (e.g., real-valued vectors) cannot be handled natively. The required conversion of continuous attributes into a finite set of discrete symbols always need a quantization step, which is inherently lossy. This directly conflicts with our framework's core principle of creating a faithful and reversible representation. Integrating continuous features in a principled manner alongside our discrete tokenization process therefore remains a key limitation.

Node and Edge Level Tasks. The current framework is primarily evaluated on graph-level prediction tasks. Adapting it for fine-grained objectives, such as node classification or link prediction, raises a general consideration for graph tokenization: the Byte Pair Encoding (BPE) process, which is essential for building an efficient vocabulary, may merge the specific target node or edge into a larger, composite token. As a result, the discrete identity of the target entity can be obscured, making it difficult to formulate a direct prediction objective.

Computational Complexity and Scalability. A key scalability limitation in our framework arises from the trade-off between different serialization methods. The Chinese Postman Problem (CPP) based approach, for instance, introduces a significant bottleneck: its $O(|\mathcal{V}|^3)$ complexity renders it impractical for datasets with large graphs. Consequently, we primarily adopt the highly efficient, linear-time `Feuler` method. With this choice, the main computational workload shifts to the BPE vocabulary training. However, this is a far more manageable constraint, as BPE training is a one-time, offline cost, and its practical runtime impact is a constant-factor consideration rather than a prohibitive asymptotic scaling issue(as detailed in Appendix B.4). A separate, downstream constraint is the Transformer's fixed context window, which limits the maximum size of a single graph. While this is an inherent limitation of the model architecture, our BPE compression significantly alleviates the issue, and adopting long-context models provides a clear path for future scaling.

A.2 Future Works

Our work opens several promising avenues for future research. Below, we outline these potential directions, ordered based on our perspective of their potential impact and research scope.

- **Graphs with Continuous Features.** To extend our framework to graphs with continuous features, a straightforward approach would be to first discretize them using methods like vector quantization (Yang et al., 2023) and then apply our pipeline. However, we argue this direction is suboptimal, as such quantization is inherently lossy and conflicts with our framework's core principle of creating a faithful, reversible representation. A more promising direction is to treat discrete and continuous information in parallel channels. For instance, features learned via message passing could be incorporated as a continuous bias added to the discrete token embeddings, analogous to how positional encodings supplement token information in standard Transformers. Alternatively, spectral graph theory offers a principled way to derive global information; the eigenvectors of the graph Laplacian could be used to generate a unique continuous encoding for each token's position within the global structure, complementing the discrete sequence.
- **Node and Edge Level Tasks.** For adapting the framework to node or edge-level tasks, an intuitive strategy might be to predict the entire composite token that contains the target entity. However, this approach is problematic as it makes the learning signal less direct and can amplify prediction errors. A more targeted and principled approach would be to modify

the BPE procedure itself. Specifically, we propose fixing the target entities so they are excluded from merging during tokenization. This would preserve the target's granularity for direct prediction, introducing an interesting trade-off between task-specific fidelity and overall vocabulary efficiency that warrants further investigation.

- **Large-Scale Pre-training and Cross-Domain Generalization.** A key advantage of our sequence-based representation is its potential for large-scale pre-training. A natural next step is to explore pre-training on large corpora of graphs from within the same domain (e.g., by combining multiple molecular datasets) to enhance in-domain performance and transferability. More ambitiously, our framework offers a new perspective on the grand challenge of cross-domain generalization. Since our method transforms any graph into a standard sequential format, we hypothesize that graphs from disparate domains can be treated as different 'languages' in NLP. Consequently, training a single, large-scale Transformer on a diverse, multi-domain corpus of tokenized graphs could facilitate unprecedented knowledge transfer, potentially giving rise to the scaling laws and unified representations that are foundational to true Graph Foundation Models. Finally, such pre-training may also serve as a novel tool for analyzing datasets. Our preliminary results suggest that a dataset's size does not always correlate with its 'information density,' and monitoring a model's overfitting on a masked prediction task could provide a new way to quantify a graph dataset's quality and diversity.

- **Further Extensions and Applications.** Our framework also opens several avenues for direct applications and algorithmic refinements. By reframing graph learning as a sequence modeling problem, it immediately enables the use of powerful autoregressive models, such as GPT-style architectures, for graph generation tasks like controllable molecular design. Furthermore, the sequential representation allows our method to seamlessly integrate with emerging long-context architectures to enhance scalability for massive graphs. Finally, a more fundamental extension could involve making the serialization process itself learnable, where traversal decisions are optimized end-to-end for a specific downstream task. While this could create a highly specialized graph-to-sequence interface, it also introduces significant challenges regarding generalization and stability.

A.3 Use of Large Language Models

In this work, we used large language models (LLMs) to assist with two non-substantive aspects of the research workflow. No part of the scientific contributions—such as algorithm design, model architecture, theoretical formulation, or experimental evaluation—was generated by or delegated to an LLM.

- **Manuscript Editing.** LLMs were used to help polish the language of the manuscript. This includes surface-level edits such as improving clarity, grammar, and conciseness of English expressions. All technical content, algorithmic designs, and empirical results were authored and validated by the authors.

- **Code Documentation and Cleanup.** At the time of open-sourcing our implementation, LLMs were used to assist in non-algorithmic tasks including: adding docstrings and inline comments, generating basic usage documentation, removing deprecated or redundant code, and improving logging output for better reproducibility. All code functionality and correctness were manually verified by the authors.

B Further Methodological Details

This section provides a formal and detailed supplement to the methodological discussions in Section 3. We aim to precisely define how classical graph traversal algorithms are adapted for the task of graph serialization, and to rigorously analyze their resulting properties of **reversibility** and **determinism**, pinpointing the exact sources of their respective strengths and weaknesses for our framework. All notations, unless specified otherwise, follow the definitions established in Section 3.1.

B.1 Formal Analysis of Node-List Serialization Methods

We first consider the class of methods that generate a sequence composed solely of node identifiers.

Formal Definition. When applied to graph serialization, a node-list traversal method is a function $f_{\text{node}} : \mathcal{G} \mapsto S$ that maps a labeled graph $\mathcal{G} = ((\mathcal{V}, \mathcal{E}), L, \Sigma)$ to a sequence of node labels $S = (s_1, s_2, \ldots, s_{|\mathcal{V}|})$. This sequence is generated by a traversal that visits every node in $\mathcal{V}$ exactly once. Let the sequence of visited nodes be $(v_1, v_2, \ldots, v_{|\mathcal{V}|})$, where $\{v_1, \ldots, v_{|\mathcal{V}|}\} = \mathcal{V}$. The output sequence is then $S = (L(v_1), L(v_2), \ldots, L(v_{|\mathcal{V}|}))$.

- For **Breadth-First Search (BFS)** and **Topological Sort**, the order of nodes in the sequence reflects the layer-by-layer or dependency-based traversal order. It is crucial to note that for $i \in [1, |\mathcal{V}| - 1]$, an edge (v_i, v_{i+1}) is not guaranteed to exist in $\mathcal{E}$.
- For **Depth-First Search (DFS)**, the standard algorithm produces a sequence where each node v_{i+1} is an unvisited neighbor of v_i (or a node reached after backtracking). The sequence of *first discovery* implies a tree structure (the DFS tree), but the output sequence itself does not encode this structure explicitly.

Reversibility. These methods are fundamentally **irreversible**. A serialization function f is reversible if, for its output $S = f(\mathcal{G})$, the set of pre-images $f^{-1}(S)$ contains a graph $\mathcal{G}'$ such that $\mathcal{G}' \cong \mathcal{G}$. For node-list methods, this condition fails. The output sequence S discards all explicit edge connectivity information. Consequently, a vast number of non-isomorphic graphs can produce the exact same node-label sequence. For example, consider two graphs on three nodes $\{A, B, C\}$ with identical labels: a path graph $\mathcal{G}_1$ with edges $\{(A, B), (B, C)\}$ and a star graph $\mathcal{G}_2$ with edges $\{(A, B), (A, C)\}$. A valid BFS starting from node A in $\mathcal{G}_1$ could produce the sequence $(L(A), L(B), L(C))$, and a BFS starting from A in $\mathcal{G}_2$ could also produce the same sequence. From the sequence alone, it is impossible to distinguish $\mathcal{G}_1$ from $\mathcal{G}_2$, thus violating reversibility.

Determinism. These methods are inherently **non-deterministic**. The source of non-determinism lies in the arbitrary selection of the next node to visit from a set of valid candidates. Formally, at any step of the traversal from a node u, let $N_{\text{valid}}(u)$ be the set of unvisited neighbors (for BFS/DFS) or nodes with no remaining incoming edges (for Topological Sort). Since $N_{\text{valid}}(u)$ is an unordered set, any choice of $v \in N_{\text{valid}}(u)$ is permissible by the standard algorithm's definition. The final sequence is thus contingent on implementation-specific details, such as the memory layout of the graph's adjacency list, which are not canonical properties of the graph itself. This leads to different sequences for the same graph, violating determinism.

B.2 Formal Analysis of Edge-Covering Serialization Methods

This class of methods generates sequences by performing a walk that traverses every edge in the graph at least once.

Formal Definition. A *walk* W in a graph $\mathcal{G}$ is a finite sequence of alternating nodes and edges, $W = (v_0, e_1, v_1, e_2, \ldots, e_k, v_k)$, where $v_i \in \mathcal{V}$, $e_i \in \mathcal{E}$, and for all $i \in [1, k]$, edge $e_i = (v_{i-1}, v_i) \in \mathcal{E}$. An edge-covering serialization function $f_{\text{edge}} : \mathcal{G} \mapsto S$ maps $\mathcal{G}$ to the label sequence corresponding to such a walk, $S = (L(v_0), L(e_1), L(v_1), \ldots, L(v_k))$, under the constraint that the multiset of edges in the walk, $\{e_1, \ldots, e_k\}$, covers the entire edge set of the graph, i.e., $\mathcal{E} \subseteq \{e_1, \ldots, e_k\}$.

- For an **Eulerian circuit**, the algorithm is applied to a graph where every undirected edge $\{u, v\} \in \mathcal{E}$ is treated as a pair of directed edges, (u, v) and (v, u), forming an edge set $\mathcal{E}'$ (Gao et al., 2025). The resulting walk traverses every edge in $\mathcal{E}'$ *exactly once*.
- For the **Chinese Postman Problem (CPP)**, the algorithm finds a walk W that covers $\mathcal{E}$ while minimizing the total weight of the walk, $\sum_{i=1}^{k} w(e_i)$, where $w(e)$ is the weight of edge e (typically 1 for unweighted graphs). This means some edges in $\mathcal{E}$ may be traversed multiple times.

Reversibility. By definition, these methods are **reversible**. The output sequence S is composed of a series of labeled triplets $(L(v_{i-1}), L(e_i), L(v_i))$. From this sequence, one can reconstruct the complete multiset of labeled edge traversals. Since this multiset is guaranteed to contain every edge from the original graph $\mathcal{E}$ at least once, the full topology of $\mathcal{G}$ can be losslessly recovered up to

isomorphism. The mapping from the graph's structure to the information contained in the sequence is injective.

Determinism. In their classical forms, these methods are **non-deterministic**.

- For an **Eulerian Path**, the non-determinism stems from Hierholzer's algorithm. At any node u during the tour construction, let $E_u^{\text{unvisited}}$ be the set of untraversed edges incident to u. The algorithm proceeds by selecting an arbitrary edge from this set. As $E_u^{\text{unvisited}}$ is an unordered set, this choice introduces ambiguity, leading to different valid Eulerian circuits and thus different output sequences.
- For the **CPP**, the primary source of non-determinism arises during the solution process. The algorithm first identifies the set of odd-degree nodes, $\mathcal{V}_{\text{odd}}$. It then computes a minimum-weight perfect matching on a complete auxiliary graph constructed on $\mathcal{V}_{\text{odd}}$. If multiple distinct perfect matchings exist that share the same minimum total weight, the choice between them is arbitrary. This choice dictates which paths in the original graph are duplicated to form an Eulerian supergraph, ultimately resulting in different minimum-cost tours and thus different sequences.

Our proposed frequency-guided mechanism (Section 3.2) addresses these specific sources of non-determinism by providing a canonical, data-driven rule for making these choices.

B.3 Disconnected Graphs

For completeness, we specify our procedure for handling graphs that are not connected. To ensure the overall serialization remains deterministic, an input graph $\mathcal{G}$ is first decomposed into its set of connected components, $\{\mathcal{G}_1, \mathcal{G}_2, \ldots, \mathcal{G}_c\}$. Each component $\mathcal{G}_i$ is independently serialized into a sequence S_i using the chosen method. The resulting set of sequences $\{S_1, \ldots, S_c\}$ is then sorted to produce a canonical ordering. The sorting criterion is primarily the length of the sequence in descending order, any ties are resolved using standard lexicographical comparison. The final output is the concatenation of these sorted sequences. This guarantees that any given graph, regardless of its connectivity, maps to a single, unique sequence.

B.4 Complexity Analysis

CPP Complexity. For CPP–based serialization, the end-to-end cost is $O(|\mathcal{V}|^3 + |\mathcal{E}|)$: $O(|\mathcal{V}|^3)$ from the minimum-weight perfect matching on odd-degree vertices, and $O(|\mathcal{E}|)$ from finding the Euler circuit after augmentation. Since $|\mathcal{E}| \leq |\mathcal{V}|^2$ (even $|\mathcal{E}| = \Theta(|\mathcal{V}|^2)$ for a complete graph), we have $O(|\mathcal{V}|^3 + |\mathcal{E}|) = O(|\mathcal{V}|^3)$, so throughout we denote the CPP family as $O(|\mathcal{V}|^3)$.

Pipeline Complexity. We analyze the computational complexity of the `GraphTokenizer` training procedure. Let $\mathcal{D} = \{\mathcal{G}_1, \ldots, \mathcal{G}_N\}$ be the training dataset, where $\mathcal{G}_i = (\mathcal{V}_i, \mathcal{E}_i)$. We define $V_S = \sum_{i=1}^{N} |\mathcal{V}_i|$ and $E_S = \sum_{i=1}^{N} |\mathcal{E}_i|$ as the total number of nodes and edges in the dataset, respectively. Let K be the number of BPE merge operations and $\bar{L}$ be the average initial sequence length, where $\bar{L} \approx E_S/N$.

Statistics Collection. This stage requires a single pass over all edges in the dataset to count local patterns. The complexity is therefore $O(E_S)$.

Graph Serialization. As summarized in Table 1, the complexity depends on the chosen method. Traversal-based methods such as `Eulerian` (and its guided variant `Feuler`) are linear in graph size, with a total cost for the dataset of $O(V_S + E_S)$. In contrast, `CPP` (and its guided variant `FCPP`) is dominated by solving a minimum-weight perfect matching for each graph, yielding a total complexity of $O(\sum_{i=1}^{N} |\mathcal{V}_i|^3)$. Assuming a relatively homogeneous distribution of graph sizes, this can be expressed as $O(N \cdot (\frac{V_S}{N})^3) = O(\frac{{V_S}^3}{N^2})$.

BPE Training. The complexity of the BPE training phase (Lines 6-14) is dominated by the sequence merge operation. For a standard implementation using dynamic arrays, the cost of a merge is proportional to sequence length. We analyze the total complexity under two bounding scenarios.

First, consider the case where a small number of pairs are merged per iteration. The work is dominated by rewriting all N sequences for each of the K iterations, leading to a total complexity of:

$$C_1 = O(K \cdot N \cdot \bar{L}) \tag{8}$$

Second, consider the case where a maximal number of pairs are merged, halving the total corpus length $n = \frac{N\bar{L}}{2}$ in each step. The work performed can be described by the recurrence relation:

$$T(n) = T(\frac{n}{2}) + f(n) \tag{9}$$

where $f(n)$ is the cost of a single merge pass. For a naive array-based merge, $f(n) = O(N \cdot (\frac{n}{N})^2) = O(\frac{n^2}{N})$. By the Master Theorem, with $a = 1, b = 2, d = 2$, we have $d > \log_b a$, so the total complexity is dominated by the root node's work:

$$C_{2,\text{naive}} = O(\frac{n^2}{N}) = O(N\bar{L}^2) \tag{10}$$

If the merge operation were optimized to be $O(1)$ per merged pair (e.g., using a linked list representation or mark new token only at range endpoint to be replaced), then $f(n) = O(n)$. In this case, $d = 1 > \log_2 1$, so the complexity would be:

$$C_{2,\text{opt}} = O(n) = O(N\bar{L}) \tag{11}$$

The final complexity depends on the termination criterion. We employ a fixed number of iterations, K, to allow for flexible control over the final vocabulary size and compression ratio across experiments. In typical settings, K (e.g., $10^3 - 10^4$) is much larger than the average sequence length $\bar{L}$ (e.g., 10^2), making the C_1 term the dominant factor. Alternatively, if one were to terminate based on a minimum frequency threshold, the process would resemble the recursive scenario, making C_2 the more relevant complexity model. Given our fixed-iteration approach, the overall BPE training complexity is:

$$C_{\text{BPE}} = O(K \cdot N \cdot \bar{L}) = \boldsymbol{O(K \cdot E_S)} \tag{12}$$

Overall Training Complexity. For serialization with `Feuler` and other method with linear time complexity, the total complexity is dominated by the BPE training, resulting in $\boldsymbol{O(K \cdot E_S)}$. If a minimum-frequency stopping criterion were used, the complexity would instead be dominated by the $C_{2,\text{naive}}$ term, becoming $O(E_S + N\bar{L}^2) = O(N\bar{L}^2) = O(\frac{E_S^2}{N})$. For serialization with `FCPP`, the total complexity is dominated by the most expensive component, yielding $\boldsymbol{O(\frac{V_S^3}{N^2} + K \cdot E_S) = O(\frac{V_S^3}{N^2})}$, which in practice for large graphs, infers that the serialization becomes bottleneck.

C Experimental Setup

This section provides the comprehensive configuration details required to fully reproduce all experiments presented in this paper.

C.1 Datasets

Our evaluation is conducted on a diverse suite of benchmark datasets. The `aqsol` and `zinc` datasets are sourced from the benchmark collection proposed by (Dwivedi et al., 2023), while the remaining datasets are standard benchmarks obtained from libraries such as PyTorch Geometric (PyG) and DGL. Table 4 below offers a comprehensive summary of their statistical properties and raw feature dimensions.

C.2 Model Architectures

We employed two Transformer backbones in our experiments. The first, which we denote as **GT+BERT**, is based on a BERT-Small architecture. The second, **GT+GTE**, utilizes a more recent and powerful GTE-Base model. The precise architectural parameters for each are detailed side-by-side in Table 5. This format facilitates direct comparison and is designed to accommodate additional model configurations in future scaling law studies. Note that the vocabulary size is determined dynamically based on the dataset and tokenization strategy, causing the total parameter count to vary slightly across experiments, the result reported here included the embedding layer size corresponding to the vocabulary encoded using BPE on the zinc dataset

Table 4: Comprehensive statistics and feature dimensions for all benchmark datasets. Node and edge counts are presented as mean ± standard deviation. "Raw Dim" refers to the dimensionality of the original features before they are mapped to discrete integer symbols.

Dataset	# Graphs	Task	# Targets	Nodes (Mean ± Std)	Edges (Mean ± Std)	Node Raw Dim	Edge Raw Dim
aqsol	9,823	Regression	1	33.7 ± 24.5	67.9 ± 50.0	65	5
coildel	3,900	Classification	100	21.5 ± 13.2	108.5 ± 77.0	2	1
colors3	10,500	Classification	11	61.3 ± 60.5	182.1 ± 187.3	4	—
dblp	19,456	Classification	2	10.5 ± 8.5	39.3 ± 39.3	1	1
dd	1,178	Classification	2	284.3 ± 272.1	1431.3 ± 1388.4	1	—
molhiv	41,127	Classification	2	25.5 ± 12.1	54.9 ± 26.4	9	3
muta	4,337	Classification	2	30.3 ± 20.1	61.5 ± 33.6	1	1
p-func	15,535	MT-Classification	10	150.9 ± 84.2	307.3 ± 172.2	9	3
p-struct	15,535	MT-Regression	11	150.9 ± 84.2	307.3 ± 172.2	9	3
proteins	1,113	Classification	2	39.1 ± 45.8	145.6 ± 169.3	2	—
qm9	130,831	Regression	16	18.0 ± 2.9	37.3 ± 6.3	16	4
synthetic	300	Classification	2	100.0 ± 0.0	392.0 ± 0.0	2	—
twitter	144,033	Classification	2	4.0 ± 1.7	10.0 ± 9.1	1	1
zinc	12,000	Regression	1	43.8 ± 8.5	91.1 ± 18.1	28	4

Table 5: Architectural parameters of the Transformer backbones used in our experiments.

Parameter	**GT+BERT**	**GT+GTE**
Model Configuration	BERT-Small	GTE-Base
Number of Hidden Layers (N)	4	12
Hidden Size (d_{model})	512	768
Number of Attention Heads (h)	4	12
FFN Intermediate Size (d_{ff})	2048	3072
Activation Function	GELU	GELU
Dropout Rate (Attention & Hidden)	0.1	0.1
Position Embedding	Learned Abs	RoPE
Max Sequence Length	768	8192
Layer Normalization ϵ	1e-12	1e-12
Total Parameters (Approx.)	$\approx$ 15M	$\approx$ 115M

C.3 Hyperparameters

Our hyperparameter tuning strategy was designed for systematic evaluation and reproducibility rather than exhaustive per-dataset optimization. We established a robust base configuration, detailed in our publicly available configuration files, which was applied to all experiments by default. For certain datasets, particularly those with very large or very small graphs, targeted adjustments were made to key parameters like batch size and learning rate to ensure stable training.

Table 6 provides a comprehensive overview of these settings. The "Default Configuration" column represents the base values applied to all datasets unless otherwise specified. The subsequent columns detail the specific overrides for datasets or groups of datasets that required adjustments. This unified view clearly illustrates both our general training strategy and the specific exceptions made.

C.4 Computational Environment

Software. Our implementation relies on a shared software stack to ensure consistency. The key packages and their versions are listed below. For a complete and exhaustive list of dependencies, please refer to the environment files in our public code repository.

- **PyTorch**: `2.1.2`
- **CUDA Toolkit**: `12.1`
- **DGL**: `2.4.0`
- **PyTorch Geometric (PyG)**: `2.4.0` (with corresponding libraries `pyg-lib`, `torch-scatter`, etc.)

Table 6: Unified hyperparameter specification. This table details the default values used for training and the specific conditions under which they were overridden.

Parameter	Default Value	Exceptions & Conditions
General Settings		
Optimizer	AdamW	—
Epochs	200	—
Weight Decay	0.1	—
Random Seed	42	—
Batch Size	32	16 on (`DBLP`, `Peptides_*`, and `COIL-DEL`)
Serialization & Tokenizer Settings		
Default Method	`Feuler`	—
BPE Enabled	True	—
BPE Merges (K)	2000	—
Finetuning Settings		
Learning Rate	1e-5	5e-5 on (`DBLP`, `molhiv`, `twitter`)
LR Warmup Ratio	0.025	—
Max Gradient Norm	0.5	—
Early Stopping	20 epochs	—
Pre-training (MLM) Settings		
Learning Rate	1e-4	5e-5 on (`muta`, `molhiv`, `qm9`, `twitter`, `dblp`) For GTE, to prevent training instability.
LR Warmup Ratio	0.12	—
Max Gradient Norm	2.0	—
Mask Probability	0.09	—

Hardware. All experiments were conducted on a heterogeneous cluster of NVIDIA GPUs, including consumer grade (GeForce RTX 2080, 3090, 4090) and data center grade (A800, H800) hardware. We verified that our results are stable and consistent across these different architectures.

D Experimental Results

This section provides supplementary results to complement the experiments presented in the main body of the paper. We include results for datasets omitted due to space constraints and provide additional ablation studies and efficiency analyses.

D.1 Qualitative Analysis and Interpretability

Visualizing the Learned Vocabulary. To understand the structural patterns captured by our tokenizer, we visualize the vocabulary constructed by BPE's merging process on the ZINC dataset. Figure 3 illustrates how BPE iteratively merges simple, frequent substructures into progressively more complex and chemically meaningful tokens.

Each row in the figure demonstrates such a merging sequence. For instance, the top row shows that a basic structure representing a sulfonyl group (`O=S=O` at 731th merge iter) is established as a token. In subsequent merge steps, BPE combines this token with adjacent atoms to form a more complex token (`C[SH](=O)=O`) and then an even larger one (`CC[SH](=O)=O`). This progression directly reflects BPE's mechanism: greedily merging the most frequent adjacent symbol pairs to build a vocabulary. Similarly, the bottom row shows the process starting from a classic benzene ring, which is then merged with neighboring carbon chains to form tokens corresponding to toluene and ethylbenzene.

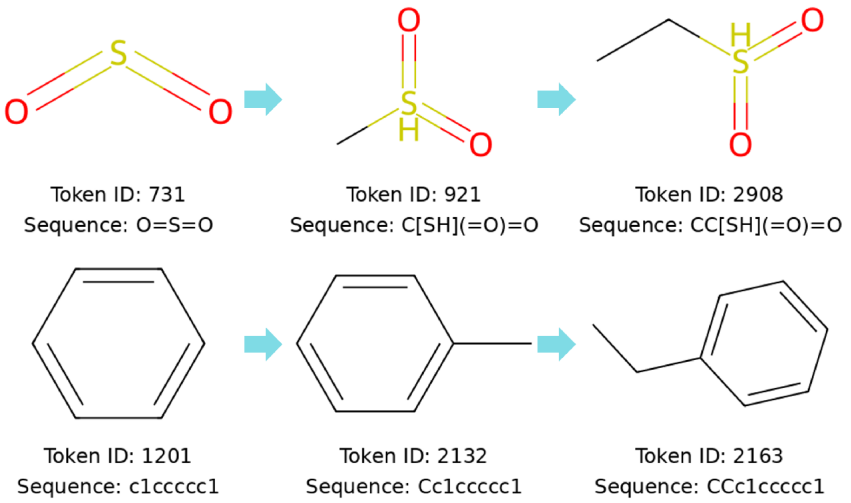

Figure 3: Illustration of the BPE merging process. Each row shows how a complex token produced by BPE merging process, demonstrating the simple substructure (left) are iteratively merged to form larger, chemically meaningful substructure (mid, and right).

Table 7: Additional classification results on datasets not shown in the main table. Best scores are in **bold**, second-best are underlined. Std in parentheses.

Model	colors3 acc↑	twitter acc↑	proteins acc↑	dd acc↑
GCN	66.0 (2.1)	52.7 (0.3)	73.2 (1.6)	62.7 (1.1)
GIN	69.3 (1.6)	55.6 (0.2)	64.3 (4.0)	65.2 (0.9)
GAT	76.6 (1.4)	53.6 (0.3)	70.5 (0.9)	58.5 (1.0)
GatedGCN	77.1 (1.2)	59.8 (0.4)	71.1 (1.2)	77.2 (0.7)
GraphGPS	77.4 (1.8)	53.0 (0.5)	67.9 (0.6)	76.3 (0.5)
Exphormer	73.9 (1.9)	55.1 (0.3)	74.1 (0.9)	74.6 (0.6)
GraphMamba	93.6 (0.9)	56.4 (0.7)	70.5 (1.1)	76.8 (0.4)
GCN+	85.8 (2.3)	61.3 (0.2)	77.1 (0.9)	79.1 (0.5)
GT+BERT	96.2 (1.7)	62.3 (0.3)	75.0 (0.7)	72.0 (0.9)
GT+GTE	**100.0** (0.0)	**65.7** (0.2)	**79.1** (0.6)	**79.6** (0.6)

D.2 Performance Results

Classification and Regression We present the complete results for all datasets evaluated in our main experiments. The experimental setup and reporting format are identical to those described in the main text. The results for the remaining datasets are detailed in Table 7.

Sequence length and efficiency. To demonstrate the generalizability of our model's efficiency, we present visualizations of token efficiency and training throughput for the remaining datasets, analogous to Figure 2 in the main paper. The results, shown in Figure 4 F̃igure 9, confirm that our approach consistently maintains superior efficiency across a diverse range of datasets.

D.3 Ablation Studies

To further validate our design choices, this section provides supplementary ablation studies that complement the analysis in the main paper. First, we extend the ablation study for the GT+GTE model in Table 8, which details the results for the remaining serialization methods and includes a specific analysis for the COLORS-3 dataset. A complete ablation study for the GT+BERT model is also presented in Table 9,Table 10. While the results are largely consistent with the trends discussed in the main paper, COLORS-3 presents a notable exception due to its unique task of counting nodes with a specific color. On this dataset, node-based serialization methods like DFS perform best as they output each node exactly once, making the counting task trivial. In contrast, our edge-traversal method can serialize a single node multiple times, which complicates direct counting. The moderate performance of GNNs is also expected, as message passing tends to diffuse the discrete one-hot

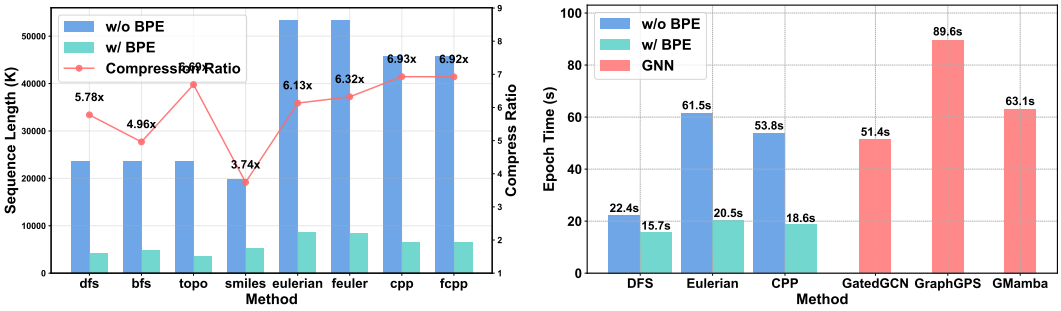

(a) Average sequence length comparison. (b) Average training time per epoch.

Figure 4: Efficiency analysis on the QM9 dataset.

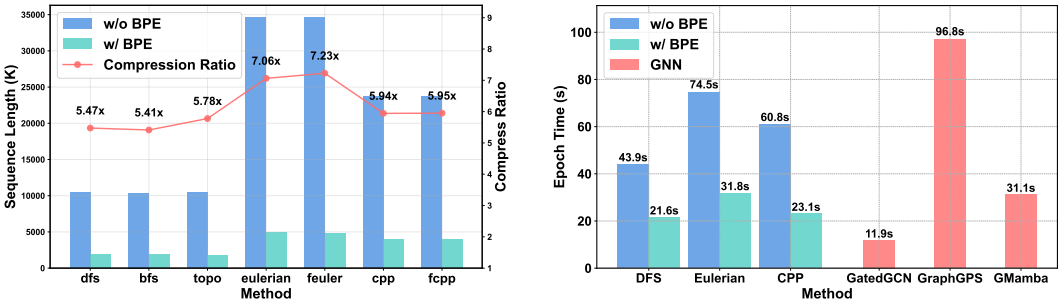

(a) Average sequence length comparison. (b) Average training time per epoch.

Figure 5: Efficiency analysis on the MolHIV dataset.

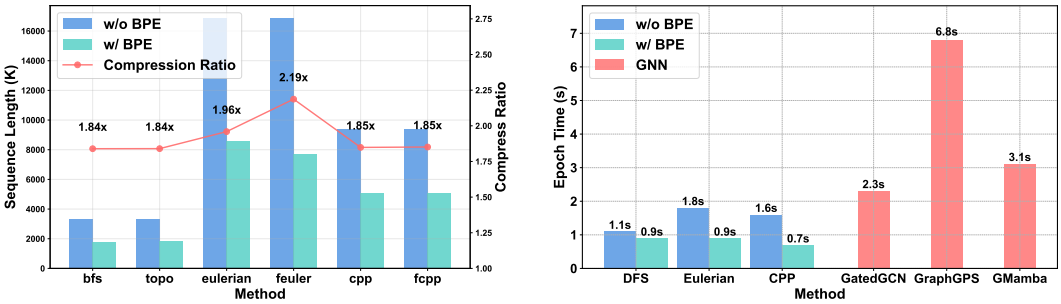

(a) Average sequence length comparison. (b) Average training time per epoch.

Figure 6: Efficiency analysis on the DD dataset.

color features, while the BPE tokenizer's node-merging strategy can obscure the node identities required for an accurate count. Despite these task-specific dynamics, a crucial finding remains consistent: our **guided** serialization method still significantly outperforms the unguided version (`w.o. guidance`), reinforcing the general effectiveness of our guidance mechanism even on tasks not perfectly aligned with the strengths of edge traversal.

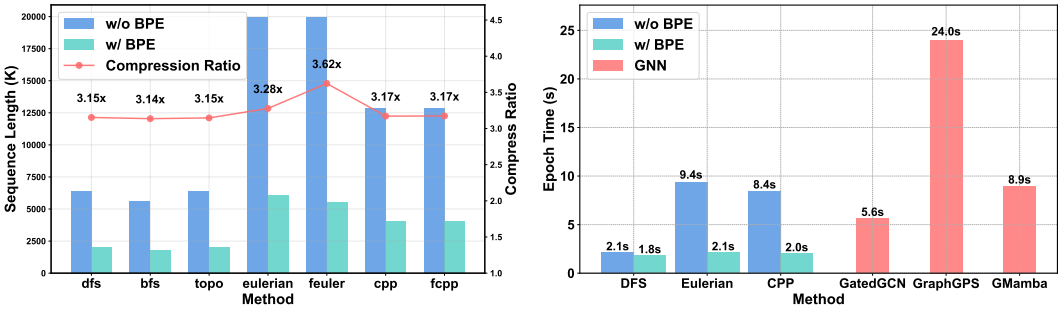

(a) Average sequence length comparison. (b) Average training time per epoch.

Figure 7: Efficiency analysis on the COLORS-3 dataset.

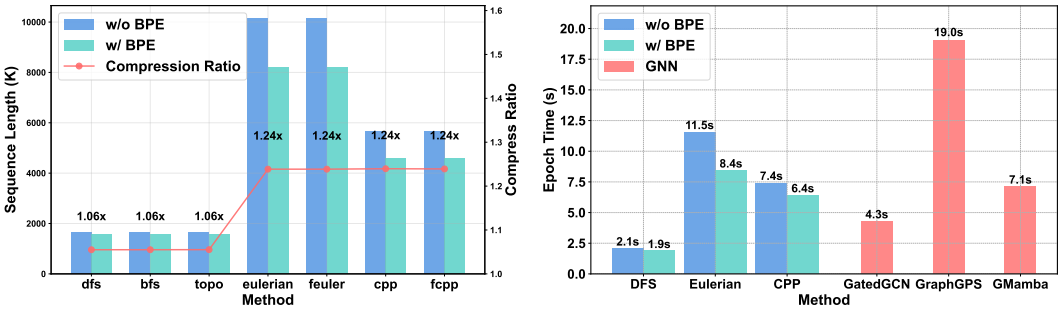

(a) Average sequence length comparison. (b) Average training time per epoch.

Figure 8: Efficiency analysis on the COIL-DEL dataset.

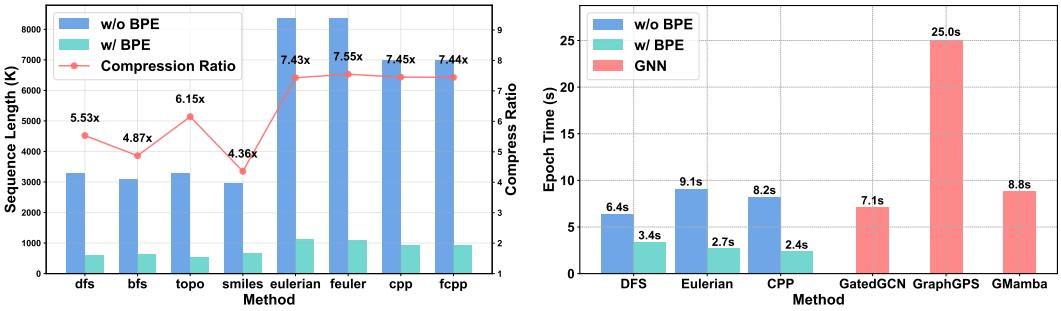

(a) Average sequence length comparison. (b) Average training time per epoch.

Figure 9: Efficiency analysis on the AQSOL dataset.

E Additional Experiments and Analysis

Note: This section contains additional experimental results and analyses conducted during the rebuttal period to address specific reviewer inquiries for clarity. The contents herein will be integrated into the main text and relevant appendices in the final revision of the paper.

E.1 Proof-of-Concept: Auto-regressive Graph Generation

A core advantage of our framework is that it converts graph data into a format formally identical to natural language, thereby theoretically enabling the use of standard autoregressive (decoder-only) models for graph generation. To empirically validate this capability, we conducted a proof-of-concept experiment using the MNIST dataset, treating images as readily visualizable grid graphs.

Table 8: Ablation with GT+GTE on additional datasets not covered in the main table. The best scores are shown in **bold**, the second-best are underlined, and standard deviations are in parentheses. A dash ("—") under SMILES indicates that the dataset either lacks SMILES representations or is not a molecular graph.

Method	mutag acc↑		colors3 acc↑		dblp acc↑		aqsol mae↓		p-struct avg mae↓	
	w	w/o	w	w/o	w	w/o	w	w/o	w	w/o
BFS	79.2 (0.9)	78.8 (0.6)	73.4 (0.8)	74.4 (0.3)	91.8 (0.19)	91.7 (0.22)	0.701 (0.017)	0.702 (0.008)	0.2495 (0.0018)	0.2494 (0.0005)
DFS	81.9 (0.7)	79.4 (1.5)	99.9 (0.1)	**100.0** (0.0)	92.8 (0.09)	92.6 (0.12)	0.684 (0.013)	0.676 (0.011)	**0.2421** (0.0026)	0.2468 (0.0040)
TOPO	80.1 (0.8)	78.4 (1.4)	76.6 (1.1)	98.3(1.3)	93.0 (0.09)	92.5 (0.13)	0.814 (0.004)	0.737 (0.003)	0.2626 (0.0022)	0.2556 (0.0002)
Eulerian	86.1 (0.9)	84.3 (1.3)	38.9 (1.0)	44.7 (2.2)	93.1 (0.09)	91.7 (0.17)	**0.609** (0.001)	0.627 (0.016)	0.2514 (0.0027)	0.2499 (0.0035)
Feuler	**90.1** (0.6)	86.7 (0.9)	41.0 (1.2)	45.3 (0.8)	**93.6** (0.08)	88.9 (0.14)	0.621 (0.007)	0.623 (0.017)	0.2510 (0.0001)	0.2548 (0.0004)
CPP	87.7 (0.8)	85.4 (0.9)	36.9 (2.4)	45.9 (1.2)	90.9 (0.14)	92.1 (0.21)	0.654 (0.016)	0.643 (0.003)	0.2535 (0.0021)	0.2482 (0.0005)
FCPP	87.7 (0.4)	86.0 (0.7)	37.5 (1.4)	45.6 (0.6)	92.4 (0.08)	92.3 (0.16)	0.654 (0.017)	0.633 (0.010)	0.2537 (0.0039)	0.2481 (0.0006)
SMILES	—	—	—	—	—	—	0.741 (0.010)	**0.673** (0.010)	—	—

Table 9: GT+BERT ablation of serialization orderings with and without BPE on main datasets. Best scores in **bold**, second-best underlined, std in parentheses. . A dash ("—") under SMILES indicates the dataset lacks SMILES or is not a molecular graph.

Method	molhiv auc↑		coildel acc↑		p-func ap↑		zinc mae↓		qm9 mae↓	
	w	w/o	w	w/o	w	w/o	w	w/o	w	w/o
BFS	76.5 (0.6)	76.1 (0.9)	81.2 (0.9)	80.1 (1.3)	66.9 (0.9)	63.2 (0.9)	0.612 (0.009)	0.961 (0.012)	0.227 (0.011)	0.324 (0.013)
DFS	74.6 (0.4)	79.5 (0.5)	80.5 (0.4)	79.8 (0.8)	**71.3** (0.3)	67.5 (1.0)	0.537 (0.008)	0.976 (0.009)	0.275 (0.009)	0.281 (0.014)
TOPO	72.2 (0.6)	77.9 (0.8)	**82.6** (0.8)	81.4 (1.2)	65.3 (0.5)	54.6 (1.0)	0.711 (0.011)	1.034 (0.012)	0.277 (0.010)	0.266 (0.011)
Eulerian	83.7 (0.7)	83.9 (1.0)	72.1 (0.6)	69.9 (2.9)	67.3 (0.9)	64.1 (1.6)	0.304 (0.008)	0.396 (0.012)	**0.104** (0.006)	0.127 (0.007)
Feuler	82.6 (0.4)	81.8 (0.5)	74.1 (0.3)	76.1 (0.9)	68.5 (1.0)	65.4 (1.1)	**0.241** (0.006)	0.432 (0.011)	0.122 (0.004)	0.128 (0.005)
CPP	**85.0** (0.3)	82.8 (0.5)	72.5 (0.5)	**83.3** (0.7)	65.6 (0.6)	59.5 (1.5)	0.319 (0.005)	0.464 (0.008)	0.115 (0.004)	0.131 (0.006)
FCPP	83.2 (0.3)	82.2 (0.6)	68.9 (0.3)	78.3 (1.0)	65.5 (1.8)	61.0 (1.2)	0.316 (0.005)	0.467 (0.007)	0.107 (0.005)	0.132 (0.007)
SMILES	—	—	—	—	—	—	0.273 (0.014)	0.320 (0.007)	0.117 (0.014)	0.120 (0.016)

Setup. We converted each 28×28 MNIST image into a regular grid graph, where pixels correspond to nodes and are connected to their immediate spatial neighbors (up, down, left, right). These grid graphs were then tokenized using our proposed framework (Frequency-Guided Serialization + BPE) to produce discrete token sequences. We trained a standard, unmodified decoder-only Transformer (GPT-style architecture) on these sequences using the conventional next-token prediction objective ($\mathcal{L}_{\text{CLM}}$).

Results. As illustrated in Figure 10, the model successfully learns to generate coherent graph structures token-by-token. The reconstructed graphs clearly depict recognizable digits, demonstrating that the model effectively captures the global topology and local connectivity patterns solely from the serialized token sequence. This result confirms that our framework effectively bridges the gap between graph generation and standard sequence modeling, opening the door for applying large-scale generative pre-training (e.g., GPT) to graph domains such as molecular design and material discovery.

E.2 Extended Comparisons with State-of-the-Art Models

We significantly expanded our comparative evaluation to include a broader range of state-of-the-art architectures and Graph Foundation Models (GFMs).

1. Broader SOTA Coverage. We conducted a comprehensive evaluation including recent Graph Transformers (**GraphGT**, **Graphormer**), serialization-based or hybrid methods (**FragNet**, **Graph-ViT-MLPMixer**), and classic baselines (**HAN**, **ChebNet**).

As shown in Table 11, our method consistently outperforms strong baselines, including specialized architectures like **FragNet** and **Graph-ViT-MLPMixer**, or generalized graph transformers like **GraphGT** or **Graphormer** on graph classification (MOLHIV, COIL-DEL) and long-range modeling tasks (Peptide-func). On the ZINC regression task, our performance is also comparable to standard Graph Transformers (e.g., **Graphormer**). And as expected, classic architectures (**ChebNet**, **HAN**) lag significantly behind modern methods. This confirms that a general-purpose tokenizer can

Table 10: GT+BERT ablation on additional datasets (Appendix). Best scores in **bold**, second-best underlined, std in parentheses. A dash ("—") under SMILES indicates the dataset lacks SMILES or is not a molecular graph.

Method	mutag acc↑		colors3 acc↑		dblp acc↑		aqsol mae↓		p-struct avg mae↓	
	w	w/o	w	w/o	w	w/o	w	w/o	w	w/o
BFS	76.1 (0.6)	76.4 (0.7)	72.7 (0.9)	67.3 (4.1)	91.9 (0.17)	91.3 (0.26)	0.851 (0.002)	0.844 (0.002)	0.2477 (0.0014)	0.2620 (0.0021)
DFS	79.6 (0.5)	77.3 (0.6)	**98.3** (0.1)	87.5 (4.4)	92.6 (0.08)	92.4 (0.13)	0.831 (0.002)	0.852 (0.002)	0.2526 (0.0036)	0.2550 (0.0012)
TOPO	74.9 (0.5)	71.2 (0.7)	60.4 (2.3)	66.6 (2.2)	92.7 (0.08)	92.7 (0.11)	0.810 (0.002)	0.840 (0.002)	0.2578 (0.0011)	0.2648 (0.0026)
Eulerian	85.5 (0.8)	82.0 (1.1)	37.8 (1.4)	40.7 (0.6)	93.1 (0.04)	91.8 (0.14)	**0.648** (0.002)	0.677 (0.003)	0.2522 (0.0012)	0.2700 (0.0049)
Feuler	**87.5** (0.4)	84.1 (0.8)	38.5 (1.1)	40.3 (1.0)	**93.2** (0.06)	88.5 (0.11)	**0.648** (0.002)	0.685 (0.004)	**0.2476** (0.0010)	0.2615 (0.0045)
CPP	85.9 (0.6)	83.6 (0.9)	36.5 (2.0)	43.5 (1.2)	90.5 (0.11)	91.7 (0.22)	0.651 (0.018)	0.690 (0.018)	0.2547 (0.0018)	0.2734 (0.0022)
FCPP	85.7 (0.5)	85.0 (0.9)	37.1 (0.6)	44.5 (1.1)	91.8 (0.13)	91.9 (0.21)	0.670 (0.005)	0.695 (0.003)	0.2541 (0.0029)	0.2681 (0.0051)
SMILES	—	—	—	—	—	—	0.746 (0.003)	0.783 (0.003)	—	—

achieve state-of-the-art performance across diverse graph learning benchmarks without specialized architectural modifications.

Table 11: Comparison with additional baselines. '*' indicates results reproduced using official implementations; '–' denotes results not reported in the original papers.

Model	ZINC (MAE ↓)	MOLHIV (AUC ↑)	Peptide-func (AP ↑)	COIL-DEL (ACC ↑)*
GraphGT	0.226 (0.014)	–	63.26 (1.26)	86.1 (0.8)
Graphormer	0.132 (0.006)	80.51 (0.53)	–	88.4 (0.3)
FragNet	0.078 (0.005)	81.32 (0.86)	66.8 (0.5)	83.4 (0.6)
Graph-ViT-MLPMixer	**0.073** (0.001)	79.97 (1.02)	69.7 (0.8)	89.1 (0.4)
HAN*	0.348 (0.042)	72.3 (0.6)	52.2 (1.1)	74.5 (0.6)
ChebNet*	0.423 (0.013)	70.1 (0.7)	51.3 (0.8)	71.4 (0.8)
Our Method	0.131 (0.007)	**87.4** (0.2)	**73.1** (0.2)	**89.6** (0.2)

2. Performance against Graph Foundation Models. We evaluated **GraphGPT** and **LLAGA** via forced adaptation (textualizing graph structures), as these models strictly require text-attributed graphs (TAGs) as input. Since standard structural benchmarks typically lack natural language attributes, we evaluated these models by treating graph features as textual tokens to satisfy their input constraints. The results in Table 12 (e.g., near-random guessing on COIL-DEL) indicate that the textualization paradigm faces significant challenges in pure structural tasks, particularly in the absence of rich semantic information.

Table 12: Performance of GraphGPT-like models via forced adaptation (Textualized Graphs). These models struggle with pure structural tasks compared to our native tokenization.

Model	ZINC (MAE ↓)	COIL-DEL (ACC ↑)
GraphGPT	0.373 (0.021)	5.6 (0.9)
LLAGA	0.317 (0.016)	12.5 (1.1)
Our Method	**0.131** (0.007)	**89.6** (0.2)

E.3 Detailed Ablation Studies and Design Validations

We conducted systematic ablation studies to validate our design choices regarding vocabulary size, frequency guidance units, and serialization strategies for counting tasks.

1. Impact of Vocabulary Size (K). Our experiments identify $K = 2000$ as the optimal saturation point for single dataset, effectively balancing sequence compression with model learnability. As shown in Table 13, increasing K initially yields significant gains in compression (1.00x to 10.84x). However, this benefit plateaus around $K = 2000$. Extending to $K = 5000$ offers diminishing returns in compression (11.34x) but fails to improve MAE (0.132). This stagnation may be driven by the "long-tail" effect: tokens added beyond $K = 2000$ appear too infrequently to receive sufficient gradient updates(even appears lower than 10 times across entire ZINC dataset), thereby increasing model complexity without contributing to generalization.

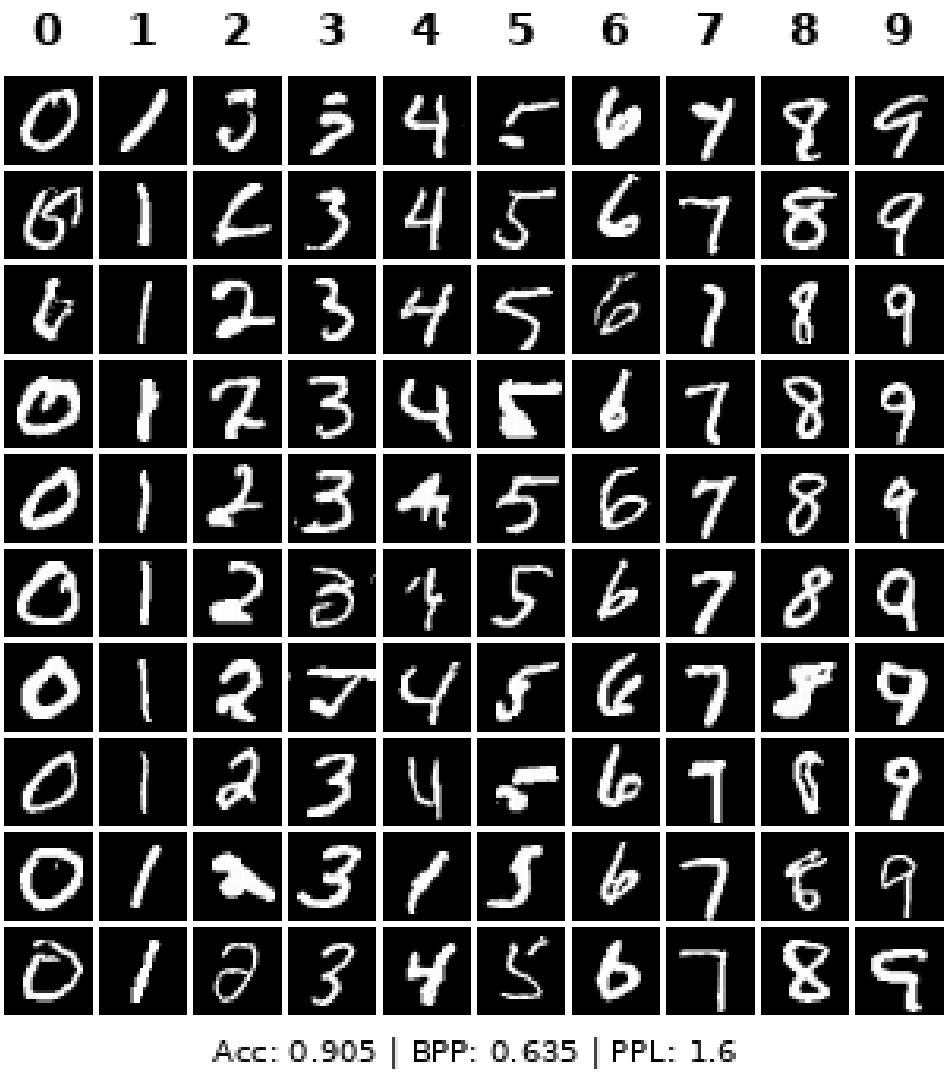

Figure 10: Visualization of autoregressive graph generation on MNIST. The model generates the graph structure token-by-token (left to right). The resulting sequences are decoded back into grid graphs, forming coherent digit images. This demonstrates the framework's capability to support generative tasks using standard decoder-only Transformers.

2. Choice of Frequency Guidance Unit. The ablation confirms that node-edge-node trigrams offer the superior trade-off, achieving the highest compression rate (10.84x) while maintaining linear complexity. The results in Table 14 show that simpler units like Node-Node bigrams perform suboptimally (10.71x) because they discard critical edge label information. Conversely, more complex units (2-hop/3-hop paths) surprisingly *reduce* compression (10.37x) despite their high computational cost ($O(E^3/N^2)$). This counter-intuitive result may be due to **data sparsity**. Specifically, as patterns grow longer, their exact recurrence becomes exponentially rarer, rendering the frequency map too sparse to provide robust global guidance.

3. Validation of Serialization Impact on Counting Tasks. The observed performance on datasets like COLORS-3 (Table 8 in main Appendix D.3) highlights the framework's flexibility. The initial performance gap arose from a mismatch between the node-counting task and our default edge-covering serialization, where repeated node visits introduce ambiguity. We validated this behavior on ZINC (counting carbon atoms) in Table 15. Switching to a DFS traversal immediately resolves

Table 13: Impact of BPE merge count (K) on compression ratio and model performance (ZINC). $K = 2000$ achieves the best balance; larger vocabularies yield diminishing compression returns and do not improve performance due to token rarity.

Merge Count (K)	Compression Ratio	Performance (MAE ↓)
0 (Raw)	1.00x	0.171 (0.013)
100	2.86x	0.144 (0.012)
500	5.37x	0.137 (0.010)
1000	8.11x	0.131 (0.011)
2000	**10.84x**	**0.131** (0.007)
5000	11.34x	0.132 (0.009)

Table 14: Impact of different statistical units on BPE compression ratio (ZINC). 'Collect Cost' denotes the complexity of gathering statistics. Trigrams achieve the highest compression with linear overhead.

Unit	Collect Cost	Compression Ratio
W/O Guidance	0	10.46x
Node-Node Bigram	$O(E)$	10.71x
Node-Edge Bigram	$O(E)$	10.72x
Node-Edge-Node Trigram	$\mathbf{O(E)}$	**10.84x**
Multi-hop Path (2 hop)	$O(E^2/N)$	10.56x
Multi-hop Path (3 hop)	$O(E^3/N^2)$	10.37x

this by ensuring unique node visits, confirming that the constraint stems from the serialization strategy rather than the Transformer architecture itself.

Table 15: Performance on simulated node counting tasks (ZINC). Switching from edge-based to node-based serialization resolves the counting failure, confirming the analysis in Appendix D.3.

Serialization Method	Accuracy (w/ BPE)	Accuracy (w/o BPE)
Edge-based (Feuler)	21.6%	24.8%
Node-based (DFS)	**83.4%**	**88.4%**

E.4 Scalability Analysis on Large-Scale OGB Datasets

To validate the scalability of our method empirically, we extended our benchmarks to include large-scale OGB datasets with millions of edges (`ogbn-arxiv`, `ogbg-code2`, and `ogbn-products`). We measured the runtime of each pipeline stage and normalized the results to **Time per 1 Million Nodes**.

As shown in Table 16, the results confirm our theoretical analysis: (1) **Linear Scalability:** The processing time remains in the order of seconds per million nodes. Even for the dense `ogbn-products` graph, serialization takes less than 30 seconds on a single CPU thread. (2) **Bottleneck Analysis:** While serialization time correlates with edge density (comparing sparse `ogbg-code2` vs. dense `ogbn-products`), the BPE encoding times remain consistently fast (ms). This confirms the efficiency of BPE as encoder.

E.5 Interpretability Analysis of Learned Vocabulary

We conducted a detailed statistical analysis of the learned vocabulary (K=2000) on the ZINC dataset to understand the BPE patterns. The results, detailed in Table 17, demonstrate that the vocabulary is not dominated by small atomic tokens. Instead, it consists primarily of composite substructures that effectively encode the graph's semantic topology.

Table 16: Efficiency of different components of our method on large-scale OGB datasets (Normalized to **Time per 1 Million Nodes**). Inference time assumes a 10x compression ratio via BPE.

Dataset	Serialization (ms)	BPE Encoding (ms)
ogbn-arxiv	14,948	57
ogbg-code2	4,108	74
ogbn-products	29,670	56

Our analysis reveals that the vocabulary exhibits a distinct preference for medium-scale patterns. As shown in Table 17, atomic tokens (0-1 nodes) constitute only **7.1%** of the vocabulary. In contrast, the distribution peaks in the **4-6 node** range (41.5%), which corresponds to the typical size of molecular functional groups and rings. Combined with the 7-9 node range, over **60%** of the vocabulary represents complex substructures. This distribution proves that BPE successfully identifies an optimal compression level-producing tokens that are large enough to capture structural context (e.g., cycles, branches) yet frequent enough to ensure generalization.

Table 17: Fine-grained distribution of token sizes (node counts) in the learned BPE vocabulary on ZINC. The distribution peaks at the 4-6 node range, indicating a preference for functional-group-sized substructures.

Token Size (Nodes)	Atomic ($0 \sim 1$)	Small ($2 \sim 3$)	**Medium** ($4 \sim 6$)	Large ($7 \sim 9$)	Huge ($10+$)
Vocabulary Proportion	7.1%	28.5%	**41.5%**	20.4%	2.5%